View metadata, citation and similar papers at core.ac.uk
brought to you by CORE
provided by NASA Technical Reports Server

AN EXPERIMENTAL INVESTIGATION OF DIELECTRIC MATERIALS FOR USE IN THIN FILM CAPACITORS

FINAL REPORT
CONTRACT NAS8-20061

SUBMITTED
BY
HOWARD E. CARR
PHYSICS DEPARTMENT
AUBURN UNIVERSITY

SUBMITTED
TO
GEORGE C. MARSHALL SPACE FLIGHT CENTER
NATIONAL AERONAUTICS AND SPACE ADMINISTRATION
HUNTSVILLE, ALABAMA 35812

January 25, 1967

ABSTRACT

An experimental survey of materials for use in thin film capacitors has been completed. Dielectric properties measured at 300°K are reported for thermally evaporated oxides 300 to 6000 angstroms in thickness of the metals Y, Sc, V, La, Ce, Pr, Nd, Sm, Gd, Dy, Ho, Er, and Yb. Thin evaporated aluminum electrodes were utilized to impress voltages in the range zero to 75 volts across the oxide layers. Dielectric breakdown strengths in excess of 5×10^6 volts/cm were observed. Relative dielectric constants measured for the oxides range from two to twenty, and measured capacitances were as high as 156×10^{-9} farads/cm^2. The oxides of Ce, La, Nd, Gd, Pr, and Er show a great deal of promise as potential materials for use in thin film capacitors. These oxides have therefore been selected for further study.

CONTENTS

I. INTRODUCTION -- 1

II. EXPERIMENTAL PROCEDURE ------------------------------------ 3

Substrate Preparation ------------------------------------ 3

Evaporation Procedure ------------------------------------ 3

Measurement -- 5

III. RESULTS -- 6

General -- 6

Geometry and Forming Properties -------------------------- 7

Dielectric and Breakdown Properties ---------------------- 8

Steady-state and Vacuum Measurements -------------------- 16

IV. CONCLUSIONS --- 18

V. SUGGESTIONS FOR FURTHER STUDY --------------------------- 20

VI. REFERENCES -- 32

TABLES

I. OXIDES INVESTIGATED, NOMINAL PURITY, AND SOURCE ------------- 22

II. TABLE OF MEASURED PROPERTIES OF THE OXIDES INVESTIGATED ----- 23

III. FIGURE OF MERIT FOR THE OXIDES INVESTIGATED ----------------- 31

FIGURE CAPTIONS

Fig. 1. Evaporation sequence and sample geometry.

Fig. 2. Circuit employed to obtain current-voltage data.

Fig. 3. Relative dielectric constant versus film thickness for neodymium oxide.

Fig. 4. Relative dielectric constant versus film thickness for gadolinium oxide.

Fig. 5. Breakdown voltage versus current-voltage cycle for capacitor Ce-1-A.

Fig. 6. Breakdown voltage versus current-voltage cycle for capacitor La-3-A.

Fig. 7. Breakdown voltage versus current-voltage cycle for capacitor Pr-1-A.

Fig. 8. Breakdown voltage versus current-voltage cycle for capacitor Nd-1-A.

Fig. 9. Breakdown voltage versus current-voltage cycle for capacitor Gd-1-A.

Fig. 10. Breakdown voltage versus current-voltage cycle for capacitor Dy-1-A.

Fig. 11. Breakdown voltage versus current-voltage cycle for capacitor Ho-3-A.

Fig. 12. Breakdown voltage versus current-voltage cycle for capacitor Er-1-B.

Fig. 13. Breakdown voltage versus current-voltage cycle for capacitor Yb-1-A.

Fig. 14. Breakdown voltage versus current-voltage cycle for capacitor Sc-1-A.

Fig. 15. Breakdown voltage versus current-voltage cycle for capacitor Y-1-C.

Fig. 16. Breakdown voltage versus current-voltage cycle for capacitor Sm-1-A.

Fig. 17. Steady-state current-voltage characteristics for capacitor Gd-3-D (oxide film thickness 1465 Å) at a pressure of 1×10^{-6} torr illustrating consistency for a number of current-voltage cycles. (The numbers on the curves correspond to the current-voltage cycle.)

Fig. 18. Steady-state current-voltage characteristics for capacitor Gd-12-A (oxide film thickness 1494 Å) at a pressure of 9×10^{-7} torr illustrating the forming process with current-voltage cycle.

Fig. 19. Steady state current-voltage characteristics for capacitor Gd-12-D (oxide film thickness 1494 Å) at a pressure of 8.2×10^{-7} torr illustrating the forming process and polarity effects. (Polarity is measured with respect to the bottom electrode).

Fig. 20. Steady-state current-voltage characteristics for capacitor Gd-17-B (thickness unknown) at a pressure of 8×10^{-7} torr illustrating polarity effects.

Fig. 21. Steady-state current-voltage characteristics for capacitor Nd-12-B (oxide film thickness 2295 Å) at a pressure of 1.6×10^{-6} torr illustrating the forming process with current-voltage cycle.

Fig. 22. Steady-state current-voltage characteristics for capacitor Nd-12-D (oxide film thickness 2295 Å) at a pressure of 1.6×10^{-6} torr illustrating the forming process with current-voltage cycle.

Fig. 23. Replot of current-voltage data of Fig. 17 for capacitor Gd-3-D illustrating linear relationship between ln(I) versus $V^{1/2}$.

Fig. 24. Replot of current-voltage data of Fig. 17 for capacitor Gd-3-D illustrating linear relationship between ln(I/V) versus $V^{1/2}$.

Fig. 25. Steady-state current-voltage characteristics for capacitor Nd-2-B (oxide film thickness 644 Å) at atmospheric pressure illustrating the forming process with current-voltage cycle.

Fig. 26. Steady-state current-voltage characteristics for capacitor Nd-11-B (thickness unknown) at atmospheric pressure illustrating the forming process with current-voltage cycle.

Fig. 27. Steady-state current-voltage characteristics for capacitor Er-2-B (thickness unknown) at atmospheric pressure.

Fig. 28. Steady-state current-voltage characteristics for capacitor Ce-1-A (oxide film thickness 6440 Å) at atmospheric pressure.

Fig 29. Steady-state current-voltage characteristics for capacitor La-3-B (oxide film thickness approximately 322 Å) at atmospheric pressure.

Fig. 30. Steady-state current-voltage characteristics for capacitor Pr-2-B (oxide film thickness 1288 Å) at atmospheric pressure.

I. INTRODUCTION

The purpose of this work was to investigate experimentally the properties of several dielectric materials for use in thin film capacitors. To date, silicon monoxide and tantalum pentoxide have been the most widely used dielectric materials for thin film applications.[1] Silicon monoxide capacitors have the advantage of stability, reproducibility, and ease of fabrication by vacuum deposition techniques. The chief disadvantages are low dielectric constant (6.0) and relatively low dielectric breakdown voltage. Tantalum pentoxide has a higher dielectric constant (25) but a lower dielectric breakdown strength, and is restricted to use in low speed circuits. To help furnish a wider variety of dielectric materials for thin film application the present experimental survey has been conducted.

During the period April 7, 1965 to October 7, 1966 the following five major tasks were performed.

1) Determine the materials to be investigated.
2) Design and build a suitable vacuum system, and assemble the necessary electronic circuitry for measurement.
3) Fabricate thin film capacitors by vacuum evaporation of the dielectric materials chosen.
4) Measure the current-voltage characteristics, dielectric breakdown strength, capacitance, and dielectric constant of these capacitors.
5) Reduce the data and evaluate the results to select the most promising materials for further investigation.

To determine the materials to be experimentally investigated, a literature survey was first conducted. The results revealed that the rare earth and transition metal oxides had many of the necessary characteristics of promising dielectric materials. Earlier work on these materials had focused on their vaporization and optical properties,[2,3,4] although some experimental work had

been aimed at determining the dielectric properties of the oxides of Yb and Dy.[5,6] The present study has proved the feasibility of evaporating thin dielectric films of these materials in a high vacuum system. The oxides investigated in this study together with the nominal purity and source of procurement are listed in Table I.

II. EXPERIMENTAL PROCEDURE

A. Substrate Preparation

The substrate chosen for fabricating the capacitors was a 3" x 1" soft-glass microscope slide. Liquid silver tabs were "fired on" to the substrate prior to evaporation by heating the slide to 600°C. Electrical contact was made to the "fired on" silver tabs by soldering copper wires with a pencil-type solder gun. This procedure was carried out prior to evaporation to avoid the possibility of heat damage to the capacitors. These contacts proved to have excellent mechanical and electrical qualities. The substrates were then vibrated in several rinses of deionized water with a Bendix ultrasonic cleaner. They were then dried in a hot air blast (approximately 100°C) for 5-10 minutes.

B. Evaporation Procedure

The vacuum system for evaporation consisted of a NRC 4" silicon oil diffusion pump backed by a 15 CFM Welch mechanical pump. The 14" x 24" pyrex bell jar was sealed to a 20" diameter stainless steel base plate by means of a viton "L" shaped gasket. Ten 1" holes were drilled on a 4" radius to accommodate high current feed-throughs for evaporation. The oxides were evaporated from tungsten boats and the electrode material was evaporated from tungsten filaments by means of the resistance heating technique. Power to the filament and boat was supplied by two step-down transformers and a Superior Electric Powerstat with a 220 volt input.

Ultimate pressure varied from 4×10^{-7} to 3×10^{-6} torr, depending on pump-down time following system exposure to air. Evaporation pressures ranged from 6×10^{-7} to 5×10^{-6} torr for the electrode material and 2×10^{-5} to 8×10^{-5} torr for the oxides. The majority of the oxides were evaporated in the upper portions of this pressure range.

The filaments, boats, oxides and electrode material were carefully outgassed prior to evaporation. To avoid contamination of the substrate and evaporated films, the substrate was shielded during outgassing. The evaporant source to substrate distance was approximately five inches. The procedure was to first evaporate a strip of aluminum $\frac{1}{8}$" by $2\frac{5}{8}$" for the base electrode. An oxide strip $\frac{1}{4}$" by $2\frac{3}{8}$" was then evaporated over the base electrode. The extra width was necessary to insure complete coverage of the base electrode, thereby eliminating the possibility of edge effects. The counterelectrodes were then evaporated over the oxide; these consisted of four aluminum strips oriented perpendicular to the base electrode. The width of these strips were $\frac{1}{4}$, $\frac{7}{32}$, $\frac{3}{16}$, and $\frac{1}{8}$", and are designated by A, B, C, and D, respectively. The distance between counterelectrodes was $\frac{11}{32}$". The fabrication sequence and sample geometry are shown in Figure 1. Three samples could be prepared in each run by utilizing a rotating stainless steel substrate holder and mask arrangement.

The temperature of the evaporant source was measured with a Leeds and Northrup optical pyrometer and found to vary from 2000 to 2300°C during evaporation of the oxides. Temperature of the substrate was monitored with an alumel-chromel type thermocouple and observed to be 25°C during deposition of electrode material and approximately 50°C during deposition of the oxides. This elevated substrate temperature was attributed to the large amount of heat necessary to accomplish evaporation of the oxides. No attempt was made to optimize on source or substrate temperature, oxide film thickness and deposition rate during capacitor fabrication. An approximate measure of the deposition rate of the oxide films was determined by calculating the ratio of film thickness to evaporation time.

C. Measurement

A schematic diagram of the circuit used to obtain current-voltage data is shown in Figure 2. Measurements were made both in vacuum and at atmospheric pressure and room temperature.

Capacitance was measured with a General Radio Company 1000 Hz general purpose bridge. The maximum error stated by the manufacturer is ±2 per cent. Oxide film thickness was measured to an accuracy of ±200 angstroms with a series MMA-MMU Metallurgical Microscope by means of the Tolansky method.[7] The capacitance formed by an insulator separated by two parallel plate conductors is expressed by

$$C = 8.842 \times 10^{-8} \frac{KA}{d}$$

where C is the capacitance in microfarads, K is the dielectric constant of the material, A is the area of the capacitor in cm^2, and d is the thickness of the dielectric in cm. Values of the dielectric constants were calculated from this formula.

III. RESULTS

A. General

The capacitors investigated were examined with a metallurgical microscope, utilizing a magnification of 400, before application of voltage across the oxide film. Immediately after removal from the vacuum system, the electrodes and exposed oxide appeared smooth and continuous. After an hour or so of exposure to normal atmospheric conditions, the exposed oxide developed dark spots and apparent discontinuities. These effects were most pronounced around the edge of the active area of a capacitor. For aluminum electrodes, such defects apparently did not have any effect on the quality of the capacitor, insofar as data taken immediately upon removal from the vacuum system did not differ markedly from that taken following an hour or so exposure to laboratory atmosphere. The characteristics obtained in vacuum, however, varied markedly from any taken at atmospheric pressure, as discussed in greater detail in Section III D. Several unsuccessful attempts were made to use copper and silver as the electrode material. For these capacitors, portions of the top electrode would disappear within an hour following removal from the vacuum system. Sufficient electrode material would ultimately disappear to give rise to an open circuit across the capacitor. It is believed that the electrode material actually diffused into the oxide.

Observations during the application of voltage revealed that dielectric breakdown in thin film capacitors occurs over a highly localized region. Breakdown is accompanied by the emission of white light and destruction of electrode material. This phenomenon was studied extensively utilizing optical microscopy techniques. No regularities with regard to size, shape, or location of such electrode destruction were noted. In general, the films were observed to recover almost immediately from the dielectric breakdown.

Some capacitors underwent such breakdown, followed by a very rapid self-healing process, a number of times without further increase in voltage. Others required 10 to 15 volts before suffering additional breakdowns following the onset of the phenomenon. Breakdown strengths are quoted in terms of the average value of the onset of the local dielectric breakdown. Further voltage cycles continued to create local breakdowns until sufficient electrode material was destroyed to give rise to an open circuit behavior.

B. Geometry and Forming Properties

Figures 3 and 4 illustrate the variation of dielectric constant with film thickness for the oxides of Nd and Gd, respectively. Each point represents the average obtained from the individual capacitors of a given sample. For Nd the trend is toward increasing dielectric constant with increasing film thickness, while for Gd there is definitely a decrease in dielectric constant with increasing film thickness. For all oxides investigated, the dielectric constant as well as the quality of the resulting capacitors was found to vary with evaporation parameters (i.e., ultimate pressure, evaporation pressure, current, and time).

Figures 5 through 16 illustrate the variation in dielectric breakdown voltage with voltage cycle number. A voltage cycle is defined as the process of increasing the voltage across the film from zero to some maximum value and then decreasing back to zero. In general, the maximum value was greater than the voltage corresponding to onset of dielectric breakdown. Several local dielectric breakdowns occur on a single voltage cycle. In general the breakdown voltage depends on the history of the capacitor, and increases with increasing voltage cycle number. Local dielectric breakdown initially

occurs at low field strengths (e.g., 0.43×10^6 V/cm for cerium oxide) and increases to some higher value (0.94×10^6 V/cm) after five or six voltage cycles. In some cases the breakdown voltage remained relatively constant, following the initial "forming" dielectric breakdowns (See Fig. 6). In other cases the breakdown voltage varied drastically following the initial breakdowns (See Fig. 10). Scandium was the only oxide which showed a decrease in breakdown voltage with increasing voltage cycle number (See Fig. 14).

C. Dielectric and Breakdown Properties

The observed properties of the oxides investigated in air are tabulated in Table II. Values of current density quoted have not been corrected for current drawn by the Moseley X-Y recorder. For values of V_{Avg} above 15 volts the correction factor is 3×10^{-4} milliampere/volt; below 15 volts, the correction factor is 1×10^{-3} milliampere/volt. The capacitors are designated by giving oxide, sample number and counterelectrode. For example, Ce-1-A refers to the capacitor formed between the base electrode and counterelectrode A from the first sample fabricated using cerium oxide as the dielectric material. Geometrical areas corresponding to the counterelectrodes are as follows:

Electrode	Geometrical area (cm^2)
A	0.2016
B	0.1764
C	0.1512
D	0.1008

Summaries of the experimental results for each oxide are given in the subsequent paragraphs.

1. Cerium

Two samples of this oxide were prepared and both revealed excellent dielectric properties. Sample number one (6440 angstroms oxide film thickness) yielded capacitance measurements on all four capacitors ranging from 3.0×10^{-9} to 5.7×10^{-9} farads. This sample had the highest average dielectric constant (19.0) of all oxides investigated. Current-voltage characteristics were relatively smooth and linear with only a few local dielectric breakdowns occurring (See Fig. 5). Sample number two (2769 angstroms) also had stable current-voltage behavior with the occurrence of only a small number of local dielectric breakdowns. Capacitance measurements were obtained on two of the capacitors from this sample with values of 1.5×10^{-9} and 1.6×10^{-9} farads. Both samples were fabricated with relative ease. Cerium oxide is the most abundant of the rare earth oxides[(8)] and shows a great deal of promise as a dielectric material for use in thin film capacitors.

2. Lanthanum

Four samples of this material were prepared, two of which were fabricated with silver electrodes (samples number one and four). No data on thickness, capacitance, or current-voltage behavior could be obtained from the samples with silver electrodes. Both samples prepared with the conventional aluminum electrodes yielded thickness measurements, the approximate values of oxide film thickness being thirteen hundred angstroms (sample No. 2) and three hundred angstroms (sample No. 3). Capacitance measurements could be obtained on only one electrode of sample number 2. The balance on the capacitance bridge was dubious and little credence could be given to this measurement and the corresponding value of the dielectric constant. Capacitance measurements were obtained on three electrodes of sample number 3 with values ranging from

6.2×10^{-9} to 20.5×10^{-9} farads. Two of the corresponding values of the dielectric constant are in close agreement (2.3 and 2.2) while the third is larger by approximately a factor of two. In general, the current-voltage characteristics show initial erratic behavior but become smoother after several voltage cycles.

3. Praseodymium

Two samples of this material were fabricated, both having an oxide film thickness of approximately thirteen hundred angstroms. Capacitance measurements were obtained on all four capacitors of both samples. These values range from 1.3×10^{-9} to 16.0×10^{-9} farads. The deposition rates varied by a factor of approximately ten for the two samples. Sample number 1 (deposition rate of 1.1 angstroms per second) yielded a lower dielectric constant (average value 1.5) but had a higher average dielectric breakdown strength (3.9×10^6 V/cm). Current-voltage characteristics for sample number 1 were initially nonlinear and erratic but became more stable and approached linearity after several voltage cycles. Sample number 2 (deposition rate of 10.1 angstroms per second) has an average dielectric constant of 12.1 and an average dielectric breakdown strength of 1.8×10^6 V/cm. One capacitor was shorted and the remaining three had current-voltage characteristics similar to sample number one. Current-voltage characteristics made between two top electrodes (two capacitors in series) on this sample were nonlinear and relatively smooth.

4. Neodymium

Fourteen samples were fabricated using neodymium oxide as the dielectric material. Nine of these samples (samples number 1, 2, 3, 4, 5, 6, 7, 9, 12) yielded thickness measurements which varied from 600 to 2300 angstroms. The corresponding values of the relative dielectric constant for the individual

capacitors varied from 7.2 to 37.6. Four samples gave consistent values of the dielectric constant, three of which indicate a value of approximately seven and the other a value of ten. The over-all average for all capacitors was found to be 12.7. Current-voltage characteristics were obtained at atmospheric pressure for samples number 1, 2, 6, and 11. These characteristics were initially erratic and linear with a positive curvature near the end of the voltage cycle. For some capacitors a pronounced nonlinear behavior was observed after 5 or 6 voltage cycles. Currents up to one milliamp at 32 volts were observed. Current-voltage data were obtained at pressures ranging from 1.2×10^{-6} to 5×10^{-6} torr for samples 6, 11, and 12. These characteristics were in general much smoother initially than those obtained at atmospheric pressure and exhibited a pronounced nonlinear behavior. Leakage currents up to one ampere at 4.4 volts were recorded in this nonlinear region. The remainder of the samples fabricated were either shorted or showed open circuit behavior and only very limited data were obtained.

5. Gadolinium

There were seventeen samples fabricated from this material. Twelve samples (samples number 1 through 5 and 8 through 14) yielded thickness measurements ranging from 600 to 2300 angstroms. Values of the relative dielectric constant range from one to above twenty for the individual capacitors with an average value of approximately eleven. Current-voltage characteristics were obtained at atmospheric pressure for samples number 1, 2, 4, 5, 8, 10, and 11. These characteristics vary from relatively smooth linear curves to nonlinear and erratic behavior. Current-voltage data at pressures below 1×10^{-6} torr were obtained for samples number 3, 12, 13, and 14. Characteristics were obtained at both atmospheric pressure and pressures below 5×10^{-6} torr

for samples number 9, 15, 16, and 17. These characteristics differ markedly. The low pressure measurements were initially smoother (See Section III D for details), and exhibit a pronounced nonlinear behavior and a higher conductivity than those obtained at atmospheric pressure.

6. Dysprosium

Five samples were fabricated from this material. Two samples (samples No. 1 and 2) yielded thickness and capacitance measurements. Current-voltage characteristics were obtained from both samples. Sample number 1 revealed an oxide film thickness of approximately 450 angstroms and a corresponding deposition rate of 0.8 angstroms per second, while the oxide film thickness of sample number 2 was 1800 angstroms and was deposited at the rate of three angstroms per second. The values of dielectric constant are consistent for the different capacitors of each sample; however, the average value for sample number 2 was 6.3, approximately twice that of sample number 1 (2.9). Sample number 2 was completely fabricated in vacuum whereas the oxide layer for sample number 1 was exposed to atmospheric pressure for approximately three hours prior to evaporation of the top electrodes. Current-voltage characteristics for sample number 1 were very erratic with dielectric breakdowns occurring at voltages as low as 0.4 volts. Current-voltage data for sample number 2 were smoother with initial dielectric breakdown occurring no lower than 14.6 volts and up to 53.6 volts.

7. Holmium

Thickness measurements were obtained on three of the six samples fabricated from this oxide with values ranging from 600 angstroms (sample number 5) to 2000 angstroms (sample number 1). Capacitance measurements varying from 2×10^{-9} to 38.1×10^{-9} farads were obtained on eight of the

corresponding 12 capacitors. Sample number 1 yielded one value of the dielectric constant (3.1); this value was approximately half that of the average value (7.7) of sample number 4, which showed reasonably consistent values. The three values of the relative dielectric constant obtained from sample number 5 are all less than one and vary by a factor of two. The balance obtained on the capacitance bridge for these capacitors was in each case questionable; therefore, little credence can be given these values. Dielectric breakdown strength was observed to vary from 0.2×10^6 V/cm up to 5.4×10^6 V/cm. Current-voltage characteristics were obtained on five samples; all of these characteristics were nonlinear with pronounced erratic behavior.

8. Erbium

Two samples were fabricated from this material. Thickness and capacitance measurements were obtained on sample number 1, the oxide film thickness being approximately 1400 angstroms. The evaporation parameters were almost identical for both samples. Capacitance values ranging from 18.2×10^{-9} to 31.2×10^{-9} farads were observed on three capacitors of sample number 2; a thickness measurement could not be obtained since no fringe shift was observed in the Tolansky interferometer. This was probably due to the thinness of the oxide film as indicated by the large capacitance measurements. Sample number 1 yielded three values of the relative dielectric constant, two of which were 3.6 and the third 2.7. Current-voltage data for this sample were essentially linear with low leakage current (26 microamperes at 40 volts for a typical capacitor). The capacitors of sample number 2 had a higher leakage current (approximately 200 microamperes at 40 volts) with a more nonlinear and erratic current-voltage behavior.

9. Ytterbium

No satisfactory capacitors were obtained from the two samples fabricated using this oxide as the dielectric material. Oxide film thickness could not be measured for either sample since no fringe shift was observed in the Tolansky interferometer. Lack of a film thickness measurement prevented making an estimate of the dielectric constant. Capacitance data were obtained on two capacitors from sample number 2 with values of 0.43×10^{-9} and 0.23×10^{-9} farads. Sample number 1 drew large currents (38 milliamperes at 20 volts) and exhibited erratic, nonlinear current-voltage behavior. Leakage current for sample number 2 was smaller (10 microamperes at 20 volts) with approximately linear current-voltage behavior over the voltage range investigated (0-75 volts).

10. Scandium

There were a total of four samples fabricated using this oxide. One attempt which proved unsuccessful utilized copper electrodes. No estimates of the dielectric constant are available due to unsuccessful attempts to measure oxide film thickness and capacitance. This material is difficult to evaporate and yielded unsatisfactory capacitors from all four samples investigated. Current-voltage characteristics were essentially linear with a pronounced erratic nature. The most interesting feature was a sharp decrease in current between 0.5 and 2 volts. Optical examination of the samples revealed electrode destruction during this transition.

11. Yttrium

One sample (sample No. 3) of the four fabricated using this oxide yielded both thickness and capacitance measurements. The oxide film thickness was 322 angstroms and capacitance values ranged from 3.4×10^{-9}

to 5.5×10^{-9} farads. The corresponding dielectric constants from this sample are in good agreement, with 1.1 being the average value. Capacitors from sample number 1 drew relatively large currents (a typical observation was 31 milliamperes at 10 volts) with an essentially linear behavior. Sample number 3 showed more erratic, nonlinear current-voltage characteristics and drew much smaller currents (10 milliamperes at 10 volts). Current-voltage data from sample number 4 were similar to that of sample number 3. All capacitors from sample number 2 were completely short-circuited. No attempt was made to remove these shorts by passage of large currents through the capacitor.

12. Vanadium

Only one sample was fabricated from this oxide due to its toxic nature. An evaporation current of only one hundred amps filled the laboratory with vapors which caused the experimentalist to become dizzy. Although the evaporation of the oxide had to be terminated, a sufficient layer of the oxide was deposited for the sample to be completed and measurements attempted the following day. Current-voltage data were obtained from two capacitors of this sample. Both showed a pronounced nonlinearity with currents up to 50 milliamperes at 5 volts. No successful measurements were made of either oxide film thickness or capacitance.

13. Samarium

Four samples were fabricated utilizing this oxide, two of which were prepared using copper as electrode material. The copper from the top electrode began to disappear quickly, following removal from the vacuum system. No film thickness or capacitance data could be obtained from these capacitors. The two remaining capacitors were fabricated using aluminum as

electrode material. No successful measurements were made on any of the resulting capacitors.

D. Steady-State and Vacuum Measurements

The current-voltage characteristics of the oxides of Nd and Gd were measured in vacuum at pressures below 5×10^{-6} torr. A terminal strip was mounted to the substrate holder allowing electrical connections to be made to the substrate inside the vacuum system. Evaporation was carried out according to standard procedure. Electrical connection to the outside test circuit was made through a NRC eight-pin instrumentation feed-through.

In general, current-voltage traces were much smoother than those measured at atmospheric pressure. The traces showed two distinct regions, a linear low-voltage region and a higher voltage region characterized by pronounced non-linearity (See Figs. 17-22). The departure from linearity occurred above approximately 1.0 volts for neodymium oxide. Currents up to 25 milliamperes were observed at this point. Maximum currents of one ampere at 6.75 volts were recorded (See Fig. 22). For gadolinium oxide the departure from linearity occurred above approximately 0.5 volts with corresponding currents up to 14.4 milliamperes. Currents up to 94 milliamperes at 8 volts were observed for this oxide in the non-linear region (See Fig. 20). The conductivity was markedly different at atmospheric pressure and for pressures below 5×10^{-6} torr. The leakage current at 3 volts and 5×10^{-7} torr was 9.3 milliamperes for capacitor Gd-15-B, whereas the current at the same voltage and atmospheric pressure was observed to be 25 microamperes. This represents a decrease in oxide conductivity by a factor of 372 with increase in pressure. Such a decrease in conductivity at atmospheric pressure was typical, although further work is necessary to establish the actual order of magnitude of the effect.

Figure 23 shows a replot of current voltage data of Fig. 17 for capacitor Gd-3-D according to ln I versus $V^{1/2}$. Note the reasonably good linear fit above 3 volts (1.76 $volts^{1/2}$ on the graph). However an equally good fit may be obtained by plotting the same data according to $\ln(I/V)$ versus $V^{1/2}$ (See Fig. 24).

Several capacitors exhibited a steady-state behavior at atmospheric pressure. That is, the current-voltage characteristics were smooth and non-linear (See Figs. 25-30). The voltage range investigated was 0 to 54 volts compared to 0 to 9 volts for the vacuum data. However, the maximum current observed (1.2 milliamperes) for the atmospheric data was much lower than that observed for the vacuum data (1 ampere). A family of curves were obtained for neodymium oxide (See Figs. 25 and 26), which are illustrative of the forming process which occurs with increasing voltage cycle. Only isolated cases of steady-state current-voltage behavior were observed for the oxides of Er, Ce, La, and Pr (See Figs. 27, 28, 29, and 30, respectively). Hence these data are not to be construed as typical behavior at atmospheric pressure for these 4 oxides. The more common observation was an erratic behavior throughout the lifetime of the capacitor. This indicates that in general the forming process did not reach completion before the electrode was totally destroyed by local dielectric breakdown. No vacuum measurements were made for these oxides.

The current-voltage data illustrated by Figs. 18-30 have not been corrected for current drawn by the X-Y recorder. For Figs. 17-22 the correction factor is 7×10^{-4} milliampere/volt with the exception of curves 34-48 of Fig. 18 and curve 18 of Fig. 19 (The numbers on the curves refer to current-voltage cycle). For these curves and the remaining figures the correction factor is 3×10^{-4} milliampere/volt.

IV. CONCLUSIONS

On the basis of the experimental survey conducted under this contract, the oxides of Ce, La, Nd, Gd, Pr, and Er show the greatest promise, and therefore, have been selected for further investigation. Cerium oxide is the most abundant of the rare earth oxides,[8] evaporates with relative ease, and has the highest average dielectric constant (19.0) of the oxides investigated. Lanthanum oxide is slightly harder to evaporate (lanthanum oxide required 180 amps through the tungsten boat compared to 150 amps for cerium oxide), but shows a tremendous dielectric breakdown strength (approximately 8.7×10^6 V/cm) and very good capacitance. Neodymium oxide has a good average dielectric breakdown strength (3.4×10^6 V/cm), high capacitance, and an average dielectric constant of 11.8, which is approximately twice that of SiO (6.0). Gadolinium oxide has a dielectric breakdown strength of the order of 3×10^6 V/cm and an average dielectric constant of 8.2. Gadolinium oxide required 193 amps for evaporation, slightly higher than the 180 amps required for neodymium oxide. Praseodymium oxide has an average dielectric breakdown strength of 3.2×10^6 V/cm and an average dielectric constant which varied with deposition rate from 1.6 for 1.1 angstroms per second to 12.1 for 10.7 angstroms per second. Erbium oxide has an average dielectric breakdown strength of 4.7×10^6 V/cm and an average dielectric constant of 3.5. Both erbium and praseodymium oxide required approximately 185 amps for evaporation.

The ratio of satisfactory capacitors (a satisfactory capacitor is one which yielded comprehensive current-voltage and capacitance data) to total number fabricated for each oxide provides a figure of merit to aid in the evaluation of the results. These figures (expressed in per cent) are tabulated in Table III. These numbers are not to be interpreted as statistically

meaningful, but are merely some measure of the worth of each oxide as a reliable dielectric material for thin film application. From Table II it can be seen that dysprosium and holmium oxide both exhibit good dielectric properties. However the difficulty experienced in evaporating these oxides along with a low figure of merit caused these oxides to be excluded from those chosen for future study.

V. SUGGESTIONS FOR FURTHER STUDY

The properties of thin film capacitors have been observed to depend, among other parameters, on oxide film thickness, evaporation pressure, deposition rate* and impurities present during evaporation.[9] Optimization of these parameters should lead to a more reliable capacitor. The first step would be to determine the functional dependence of dielectric constant, breakdown strength, and the overall performance of a capacitor on each of these parameters. The approach should be to vary the parameters one at a time, holding all others fixed. The role of deposition rate could be determined by fixing the oxide film thickness and varying the evaporation time, thereby varying the deposition rate. This would require a deposition rate controller and monitor. The experiment would need to be performed in an ultra-high vacuum system so as to reduce to a minimum the amount of impurities present during evaporation. The role of impurities could be determined by pumping the vacuum system to 10^{-10} torr or lower and then introducing a selected gas into the system to a partial pressure similar to the background partial pressure of this particular gas in a conventional 10^{-6} torr evaporator. Evaporation and subsequent measurement would then be carried out according to standard procedure.

A general lack of understanding of the current transport and dielectric breakdown mechanisms in thin film capacitors suggest the initiation of further basic experiments along these lines. A particularly fruitful experiment would be to determine the gaseous and solid products given off from a capacitor during breakdown. This could be accomplished by continously monitoring with a quadrapole residual gas analyzer the gases ejected into an ultra-high vacuum during dielectric breakdown. The ultra-high vacuum system is necessary to

---

*See Table II.

prevent background gases from masking the volatile decomposition products of dielectric breakdown. Following breakdown, the neighborhood of the breakdown spot should be analyzed using x-ray diffraction techniques to ascertain the degree to which the oxide and electrode material have crystallized, recrystallized, or chemically reacted. The role of conduction channels, heating, and subsequent decomposition of the dielectric material should be clarified by such experiments.

TABLE I

OXIDES INVESTIGATED, NOMINAL PURITY, AND SOURCE

Oxide	Purity (%)	Source
Scandium	99.9	a
Vanadium	99.9	b
Yttrium	99.9	a
Lanthanum	99.0	c
Cerium	99.9	a
Praseodymium	99.9	a
Neodymium	99.9	a
Samarium	99.9	c
Gadolinium	99.9	a
Dysprosium	99.9	a
Holmium	99.9	a
Erbium	99.9	a
Ytterbium	99.9	a

a. Bernard Ring Inc.
239 Park Avenue South
New York, New York 10003

b. Gallard Schlesinger Mfg. Corp.
Carle Place, New York

c. Electronic Space Products, Inc.
854 So. Robertson Blvd.
Los Angeles, California 90035

TABLE II

TABLE OF MEASURED PROPERTIES OF THE OXIDES INVESTIGATED

Oxide	Oxide Film Thickness (± 200 Å)	Capacitor Number	Deposition Rate (Å/sec)	V_L Low Breakdown Voltage (Volts)	V_H High Breakdown Voltage (Volts)	V_{Avg} Average Breakdown Voltage (Volts)	Dielectric Breakdown Strength Corresponding to V_{Avg} (10^5 V/cm) (±20%)	Leakage Current Density Corresponding To V_{Avg} (ma/cm^2)	Capacitance (10^{-9} Farads) (±2%)	Dissipation Factor	Dielectric Constant (±22%)	Comments*
Ce	6440	1-A	5.4	28.1	63.8	60.5	0.94	0.06-0.15	5.7	0.27	20.6	
Ce	6440	1-B	5.4	30.5	30.5	30.5	0.47	0.09-0.28	3.3	0.21	13.6	a
Ce	6440	1-C	5.4	8.8	55.5	50.0	0.78	0.18-0.50	3.0	0.22	14.4	
Ce	6440	1-D	5.4	54.5	63.5	59.0	0.92	0.32-1.1	3.8	0.27	27.4	
Ce	2769	2-A	92.0	>75.0	>75.0	>75.0	>2.7		1.5	0.20	2.3	b
Ce	2769	2-B	92.0	>64.2	>64.2	>64.2	>2.3		1.6	0.21	2.8	b
Ce	2769	2-C	92.0	>63.8	>63.8	>63.8	>2.3					b,c

*Comments

a - Only one breakdown observed
b - No breakdowns observed up to maximum applied voltage
c - No balance obtainable on capacitance bridge
d - Balance on capacitance bridge questionable
e - Short circuit behavior
f - Open circuit behavior
g - No fringe shift observed in Tolansky interferometer

TABLE II. (Continued)

Oxide	Oxide Film Thickness (± 200 Å)	Capacitor Number	Deposition Rate (Å/sec)	V_L Low Breakdown Voltage (Volts)	V_H High Breakdown Voltage (Volts)	V_{Avg} Average Breakdown Voltage (Volts)	Dielectric Breakdown Strength Corresponding To V_{Avg} (10^6V/cm) (±20%)	Leakage Current Density Corresponding To V_{Avg} (ma/cm^2)	Capacitance (10^{-9} Farads) (±2%)	Dissipation Factor	Dielectric Constant (±22%)	Comments
La	322	3-A	1.0	2.5	27.8	25.6	7.9	1.2 -1.5				c
La	322	3-B	1.0	8.2	33.5	27.2	8.9	0.23-1.9	11.0	0.14	2.3	
La	322	3-C	1.0	0.4	29.2	27.1	8.9	0.36-2.2	20.5	0.15	4.9	
La	322	3-D	1.0	16.8	71.8	29.4	8.9	0.45-0.55	6.2	0.28	2.2	
							8.7				3.1	
Pr	1265	1-A	1.1	2.5	60.8	53.6	4.2	0.22-0.65	2.4	0.22	1.7	
Pr	1265	1-B	1.1	8.4	58.8	41.0	3.2	0.12-0.45	5.4	0.21	4.4	c
Pr	1265	1-C	1.1	11.2	62.6	51.0	4.0	0.18-0.40	1.1	0.19	1.0	
Pr	1265	1-D	1.1	5.8	59.8	42.1	3.3	0.20-0.65	1.3	0.20	1.8	
Pr	1288	2-A	10.7	26.4	40.3	34.3	2.7	0.29-0.40	16.0	0.04	11.6	
Pr	1288	2-B	10.7	22.2	22.2	22.2	1.7	0.10-0.17	15.0	0.04	12.4	a
Pr	1288	2-C	10.7						12.2	0.05	11.7	e
Pr	1288	2-D	10.7	12.2	12.2	12.2	0.95	0.31-0.34	8.7	0.08	12.6	a

TABLE II. (Continued)

Oxide	Oxide Film Thickness (± 200 Å)	Capacitor Number	Deposition Rate (Å/sec)	V_L Low Breakdown Voltage (Volts)	V_H High Breakdown Voltage (Volts)	V_{Avg} Average Breakdown Voltage (Volts)	Dielectric Breakdown Strength Corresponding To V_{Avg} (10^6V/cm) (±20%)	Leakage Current Density Corresponding To V_{Avg} (ma/cm^2)	Capacitance (10^{-9} Farads) (±2%)	Dissipation Factor	Dielectric Constant (±22%)	Comments
Nd	955	1-A	15.9	7.8	60.0	54.6	5.7	0.13-0.25	14.9	0.04	8.0	
Nd	955	1-B	15.9	12.2	59.6	48.2	5.0	0.11-2.1	14.1	0.05	8.6	
Nd	955	1-C	15.9	22.6	61.5	50.3	5.3	0.14-2.0	11.9	0.04	8.5	
Nd	955	1-D	15.9									e
Nd	644	2-A	10.7	0.4	4.3	3.1	0.5	0.40-1.1	31.2	0.18	11.2	
Nd	644	2-B	10.7	3.4	27.8	13.1	2.0	0.13-0.18	25.0	0.13	10.3	
Nd	644	2-C	10.7	7.7	42.0	20.1	3.1	0.24-0.43	20.4	0.12	9.8	
Nd	644	2-D	10.7	5.5	48.0	14.8	2.3	0.20-1.9	13.9	0.15	10.1	
											9.5+	
Gd	2254	1-A	37.5	46.6	70.1	62.6	2.8	0.19-0.20	8.7	0.01	10.7	
Gd	2254	1-B	37.5	42.3	74.0	64.9	2.9	0.17-0.22	8.9	0.01	12.8	
Gd	2254	1-C	37.5	>75.0	>75.0	>75.0	>3.3		7.0	0.01	11.7	b
Gd	2254	1-D	37.5									f
											11.7	

+The quantities within the double lines represent average values.

TABLE II. (Continued)

Oxide	Oxide Film Thickness (± 200 Å)	Capacitor Number	Deposition Rate (Å/sec)	V_L Low Breakdown Voltage (Volts)	V_H High Breakdown Voltage (Volts)	V_{Avg} Average Breakdown Voltage (Volts)	Dielectric Breakdown Strength Corresponding To V_{Avg} (10^6V/cm) (±20%)	Leakage Current Density Corresponding To V_{Avg} (ma/cm^2)	Capacitance (10^{-9} Farads) (±2%)	Dissipation Factor	Dielectric Constant (±22%)	Comments
Dy	460	1-A	0.8	4.6	33.8	13.1	2.9	0.04-0.07	11.0	0.03	2.9	
Dy	460	1-B	0.8	0.3	50.0	26.6	5.8	0.27-0.44	9.8	0.02	2.9	
Dy	460	1-C	0.8	0.5	52.7	29.9	6.5	0.28-0.53	8.5	0.02	2.9	
Dy	460	1-D	0.8	0.2	14.9	8.5	1.8	0.04-0.07	6.0	0.03	3.1	
Dy	1795	2-A	3.0	53.5	75.0	65.6	3.6	0.21-0.24	6.2	0.01	6.3	
Dy	1795	2-B	3.0	53.6	75.0	66.3	3.7	0.24-0.29	5.8	0.01	6.7	
Dy	1795	2-C	3.0	14.6	74.8	67.7	3.8	0.28-3.0	4.6	0.01	6.2	
Dy	1795	2-D	3.0	53.3	74.8	64.9	3.6	0.41-0.47	3.0	0.01	6.0	
											4.6	

TABLE II. (Continued)

Oxide	Oxide Film Thickness (± 200 Å)	Capacitor Number	Deposition Rate (Å/sec)	V_L Low Breakdown Voltage (Volts)	V_H High Breakdown Voltage (Volts)	V_{Avg} Average Breakdown Voltage (Volts)	Dielectric Breakdown Strength Corresponding To V_{Avg} (10^6V/cm) (±20%)	Leakage Current Density Corresponding To V_{Avg} (ma/cm^2)	Capacitance (10^{-9} Farads) (±2%)	Dissipation Factor	Dielectric Constant (±22%)	Comments
Ho	1992	1-A	6.6									e
Ho	1992	1-B	6.6	1.3	7.4	4.8	0.2	0.02-0.5	2.39	0.08	3.0	
Ho	1992	1-C	6.6									e
Ho	1992	1-D	6.6	2.7	66.2	6.2	0.3	0.04-0.11				c
Ho	1073	4-A	6.1	0.5	11.1	4.0	0.4	0.02-0.09	12.5	0.07	7.6	
Ho	1073	4-B	6.1	5.8	73.9	53.3	5.0	0.17-2.7	11.4	0.07	7.9	
Ho	1073	4-C	6.1	20.6	75.0	57.8	5.4	0.23-2.9	9.4	0.06	7.5	
Ho	1073	4-D	6.1	1.0	68.8	38.6	3.6	0.20-2.4	6.5	0.08	7.8	
											7.7	
Er	1380	1-A	15.3	>30	>30	>30	>2.2		4.6	0.02	3.6	b
Er	1380	1-B	15.3	28.1	74.7	64.1	4.7	0.24-0.32	3.0	0.02	2.7	
Er	1380	1-C	15.3	42.7	74.7	67.1	4.9	0.30-0.36	3.6	0.02	3.7	
Er	1380	1-D	15.3	36.3	73.6	62.1	4.5	0.25-0.33				c

TABLE II. (Continued)

Oxide	Oxide Film Thickness (± 200 Å)	Capacitor Number	Deposition Rate (Å/sec)	V_L Low Breakdown Voltage (Volts)	V_H High Breakdown Voltage (Volts)	V_{Avg} Average Breakdown Voltage (Volts)	Dielectric Breakdown Strength Corresponding To V_{Avg} (10^6V/cm) (±20%)	Leakage Current Density Corresponding To V_{Avg} (ma/cm^2)	Capacitance (10^{-9} Farads) (±2%)	Dissipation Factor	Dielectric Constant (±22%)	Comments
Yb		2-A										f,g
Yb		2-B		25.5	73.2	49.9		0.21- 0.45	0.42	0.22		g
Yb		2-C		7.4	11.9	9.6		0.06- 0.16	0.43	0.15		g
Yb		2-D		8.4	12.1	10.3		0.05- 0.12				e,g
Sc		1-A		0.04	7.4	1.4		0.25- 43.0				c,g
Sc		1-B										g
Sc		1-C		0.2	5.0	1.1		0.66- 6.1				c,g
Sc		1-D		0.3	5.3	1.5		0.10- 57.0	0.8	0.10		g
Sc		2-A										e,g
Sc		2-B										e,g
Sc		2-C		0.6	22.8	2.5		0.06- 3.3	5.2	0.11		g
Sc		2-D		0.3	14.0	0.6		0.10-150	4.2	0.10		g

TABLE II. (Continued)

Oxide	Oxide Film Thickness (± 200 Å)	Capacitor Number	Deposition Rate (Å/sec)	V_L Low Breakdown Voltage (Volts)	V_H High Breakdown Voltage (Volts)	V_{Avg} Average Breakdown Voltage (Volts)	Dielectric Breakdown Strength Corresponding To V_{Avg} (10^6V/cm) (±20%)	Leakage Current Density Corresponding To V_{Avg} (ma/cm^2)	Capacitance (10^{-9} Farads) (±2%)	Dissipation Factor	Dielectric Constant (±22%)	Comments
Y		1-A										g
Y		1-B		0.4	24.9	7.4		0.17- 7.9	0.01	0.22		g
Y		1-C		0.6	22.0	6.1		0.06- 1.0	0.009	0.23		g
Y		1-D		0.4	13.8	3.2		0.10-11.0	0.01	0.21		g
Y	322	3-A	5.4	2.2	28.6	14.2	4.4	0.07- 0.25	5.5	0.05	1.0	
Y	322	3-B	5.4	0.1	46.5	8.9	2.8	0.05- 0.19	5.2	0.06	1.1	
Y	322	3-C	5.4	1.8	44.0	16.8	5.2	0.05- 0.07	4.2	0.05	1.0	
Y	322	3-D	5.4	12.1	39.5	20.9	6.5	0.12- 0.24	3.4	0.06	1.2	
V		1-A										b,c,g
V		1-B		0.9	1.8	1.4		5.7 -91.0				c,g
V		1-C										e,g
V		1-D										e,g

TABLE II. (Continued)

Oxide	Oxide Film Thickness (± 200 Å)	Capacitor Number	Deposition Rate (Å/sec)	V_L Low Breakdown Voltage (Volts)	V_H High Breakdown Voltage (Volts)	V_{Avg} Average Breakdown Voltage (Volts)	Dielectric Breakdown Strength Corresponding to V_{Avg} (10^6V/cm) (±20%)	Leakage Current Density Corresponding To V_{Avg} (ma/cm^2)	Capacitance (10^{-9} Farads) (±2%)	Dissipation Factor	Dielectric Constant (±22%)	Comments
Sm		1-A		0.4	38.5	15.0		0.05-0.20				c,g
Sm		1-B		0.7	14.7	11.1		0.11-2.8				c,g
Sm		1-C		0.5	69.2	21.0		0.13-0.17				c,g
Sm		1-D		29.9	64.7	43.5		2.8 -4.2				c,g

TABLE III

FIGURE OF MERIT* FOR THE OXIDES INVESTIGATED

Oxide	Figure of Merit (%)
Ce	75
La	62
Pr	100
Nd	71
Gd	88
Dy	40
Ho	33
Er	88
Yb	0
Sc	0
Y	25
V	0
Sm	0

* Figure of Merit is defined as the ratio of satisfactory capacitors to total number of capacitors fabricated. A satisfactory capacitor is one which yielded capacitance and current-voltage measurements. These numbers are not intended to be statistically meaningful, but are included merely as some measure of the worth of each oxide as a reliable dielectric material when prepared under our experimental conditions.

VI. REFERENCES

1. F. W. Schenkel, Electronics, January 25, 1965, p. 67.

2. M. B. Panish, J. Chem. Phys. 34, 1079 (1961); 34, 2197 (1961).

3. P. N. Walsh, H. W. Goldstein, D. White, J. Am. Ceram. Soc. 43, 229 (1960).

4. G. Hass, J. B. Ramsey, and R. Thun, J. Opt. Soc. Am. 49, 116 (1959).

5. C. Feldman and M. Hacskaylo, Rev. Sci. Instr. 33, 1459 (1962).

6. M. Hacskaylo and R. C. Smith, J. Appl. Phys. 37, 1767 (1966).

7. S. Tolansky, Multiple Beam Interferometry of Surfaces and Films (Oxford University Press, London, 1945) p. 224.

8. W. L. Silvernail and R. M. Healy, Cerium (A report prepared for the Encyclopedia of Chemical Technology by American Potash and Chemical Corporation, West Chicago, Illinois, 1963) p. 2.

9. L. Holland, Vacuum Deposition of Thin Films (Chapman and Hall, Ltd., London, 1963).

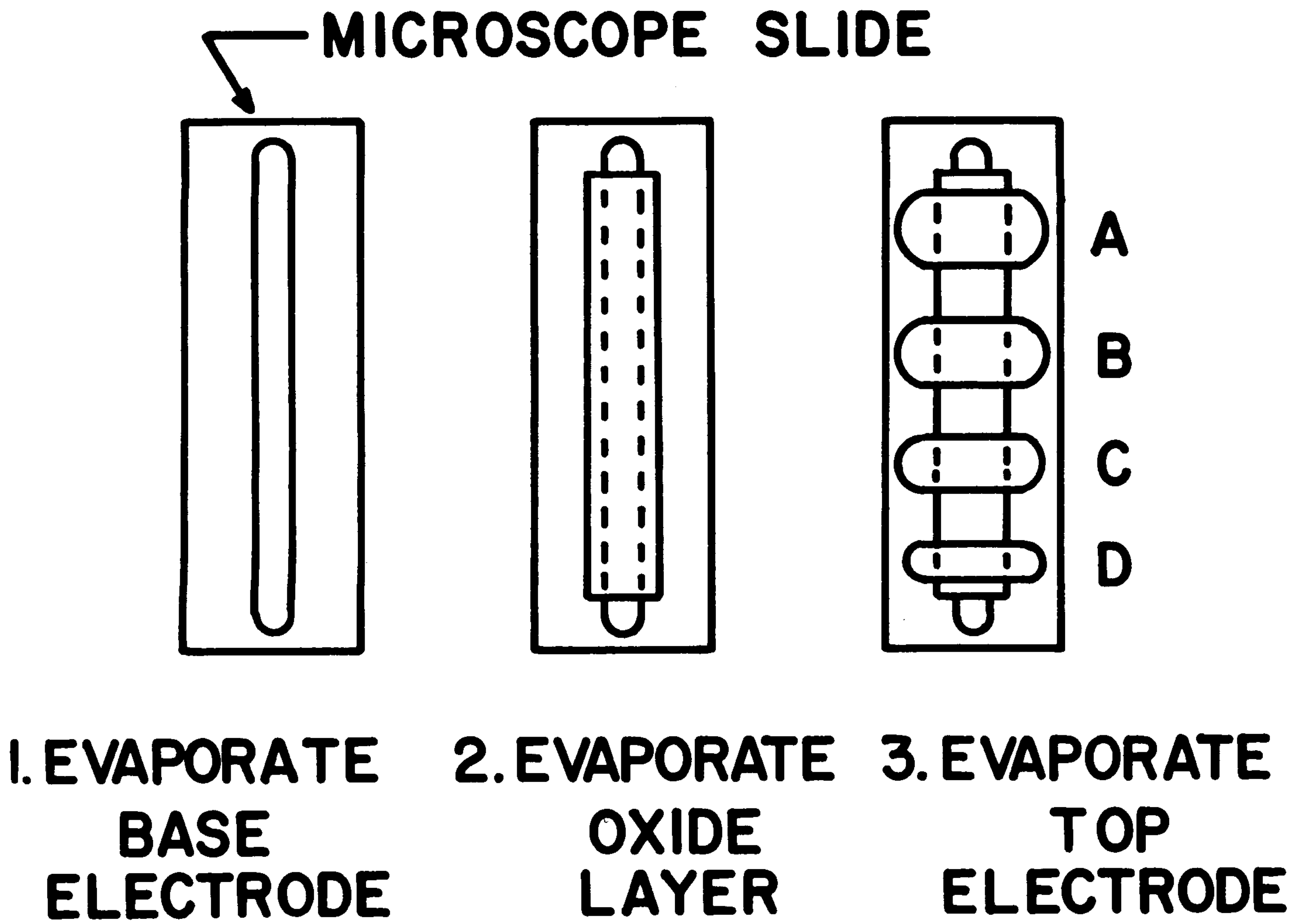

Fig. 1. Evaporation sequence and sample geometry.

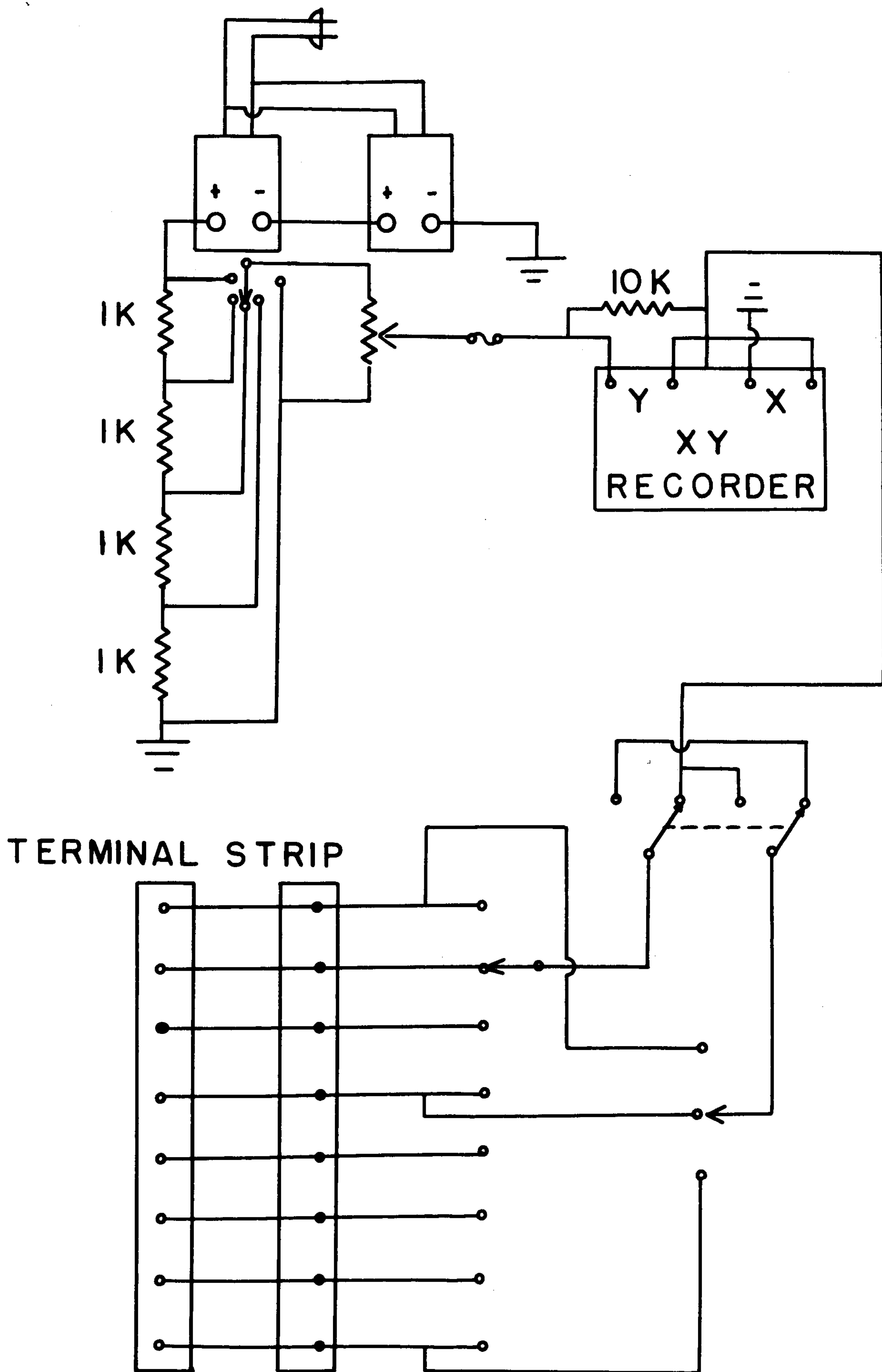

Fig. 2. Circuit employed to obtain current-voltage data.

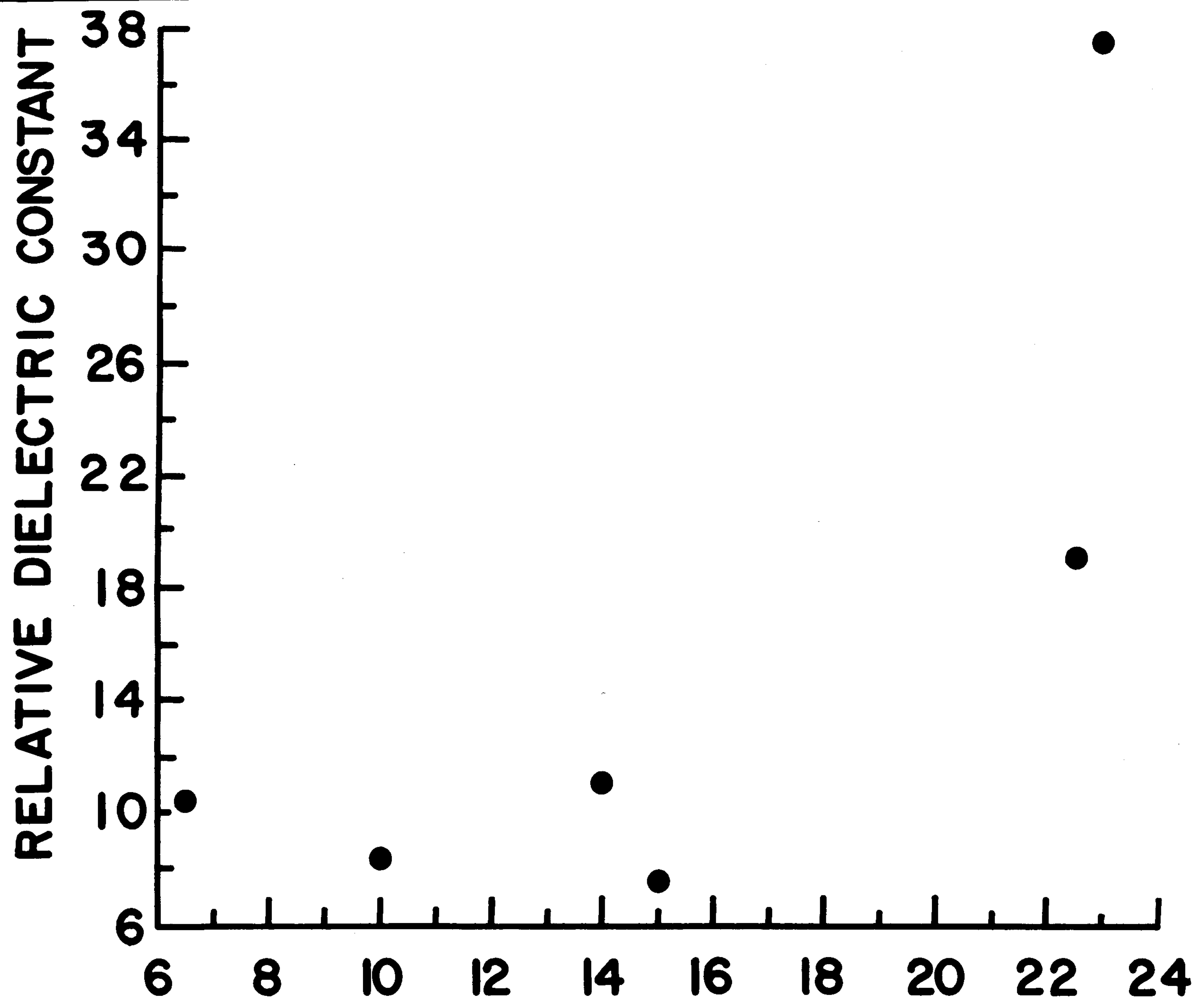

Fig. 3. Relative dielectric constant versus film thickness for neodymium

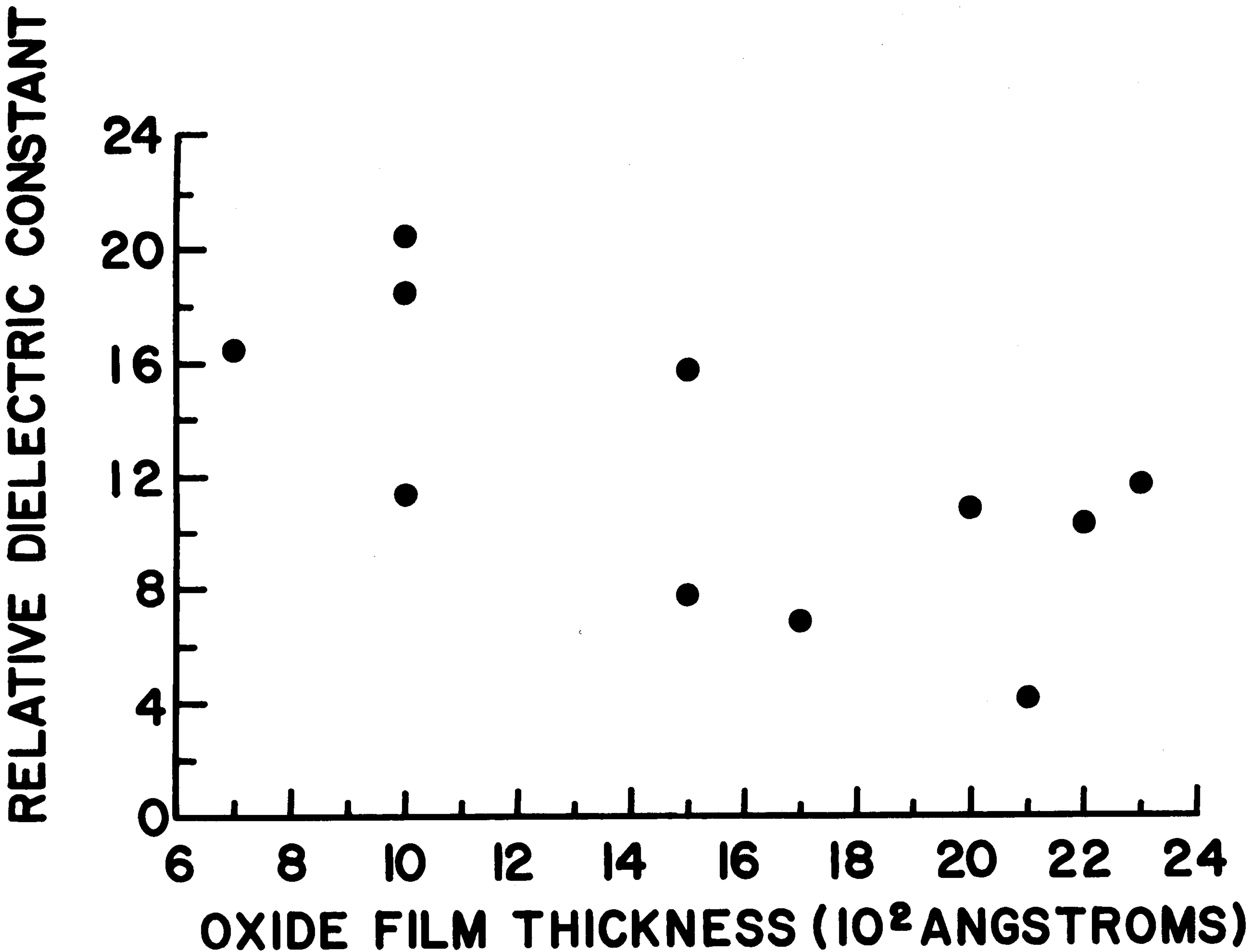

Fig. 4. Relative dielectric constant versus film thickness for gadolinium oxide.

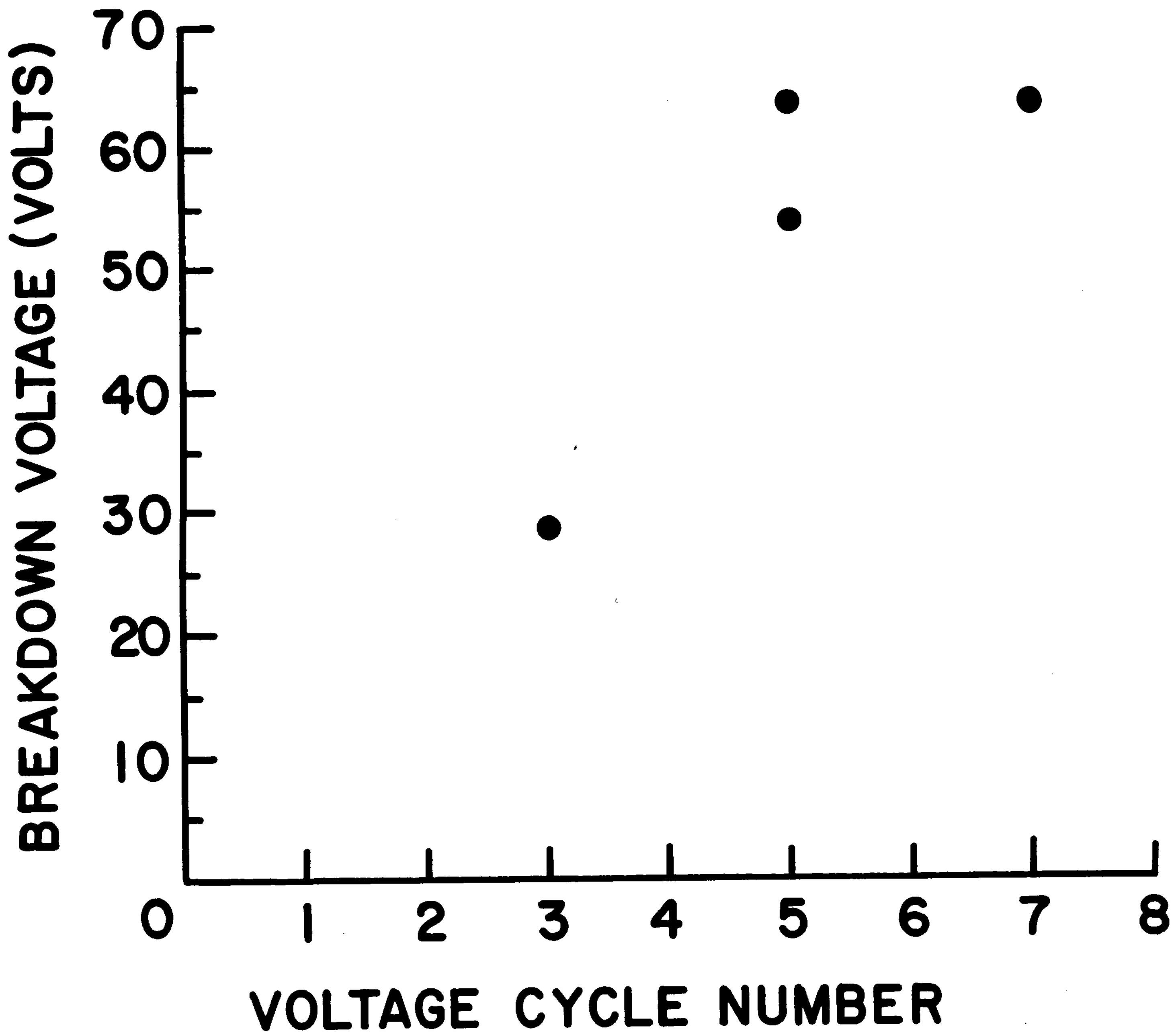

Fig. 5. Breakdown voltage versus current-voltage cycle for capacitor Ce-1-A.

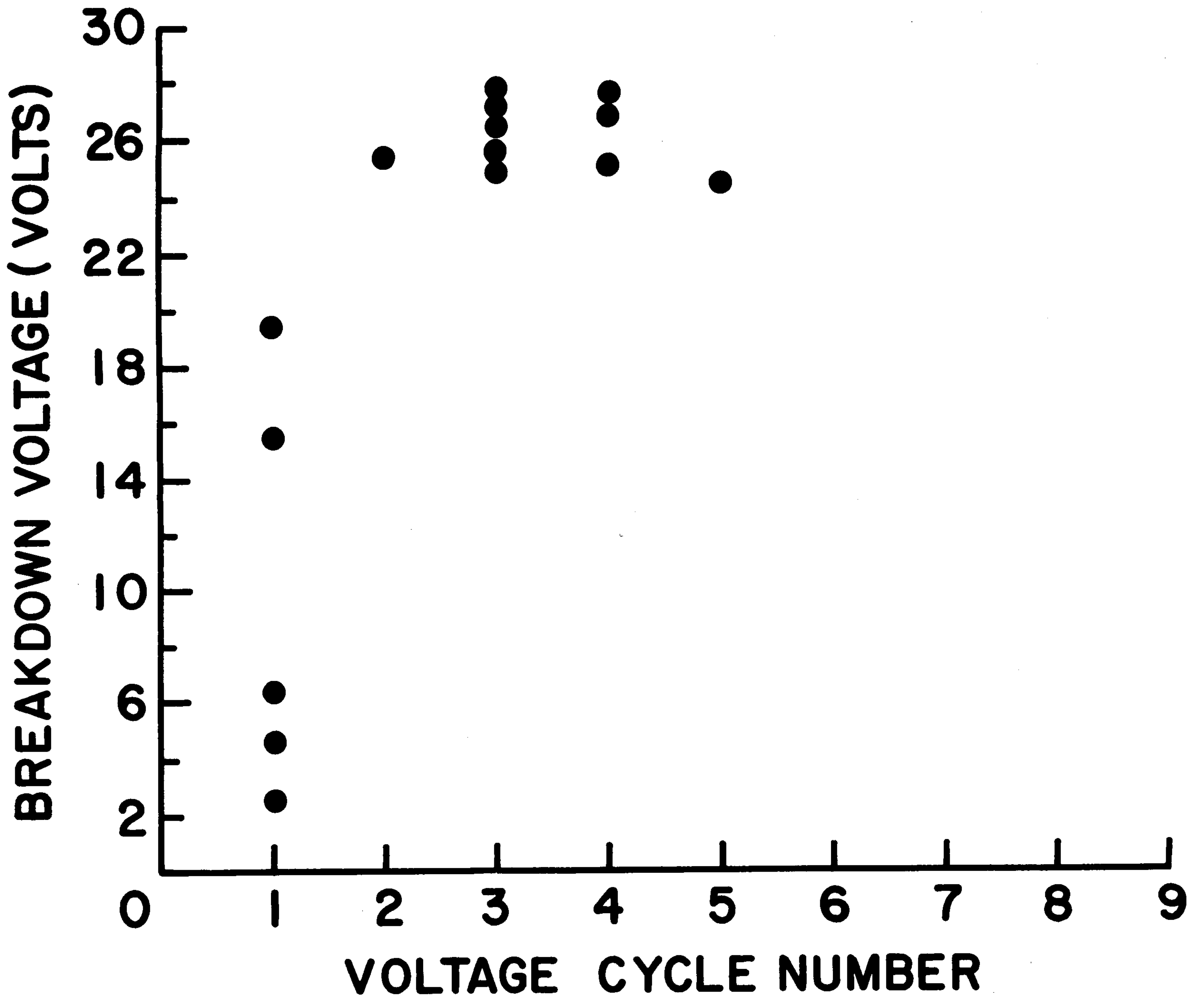

Fig. 6. Breakdown voltage versus current-voltage cycle for capacitor La-3-A.

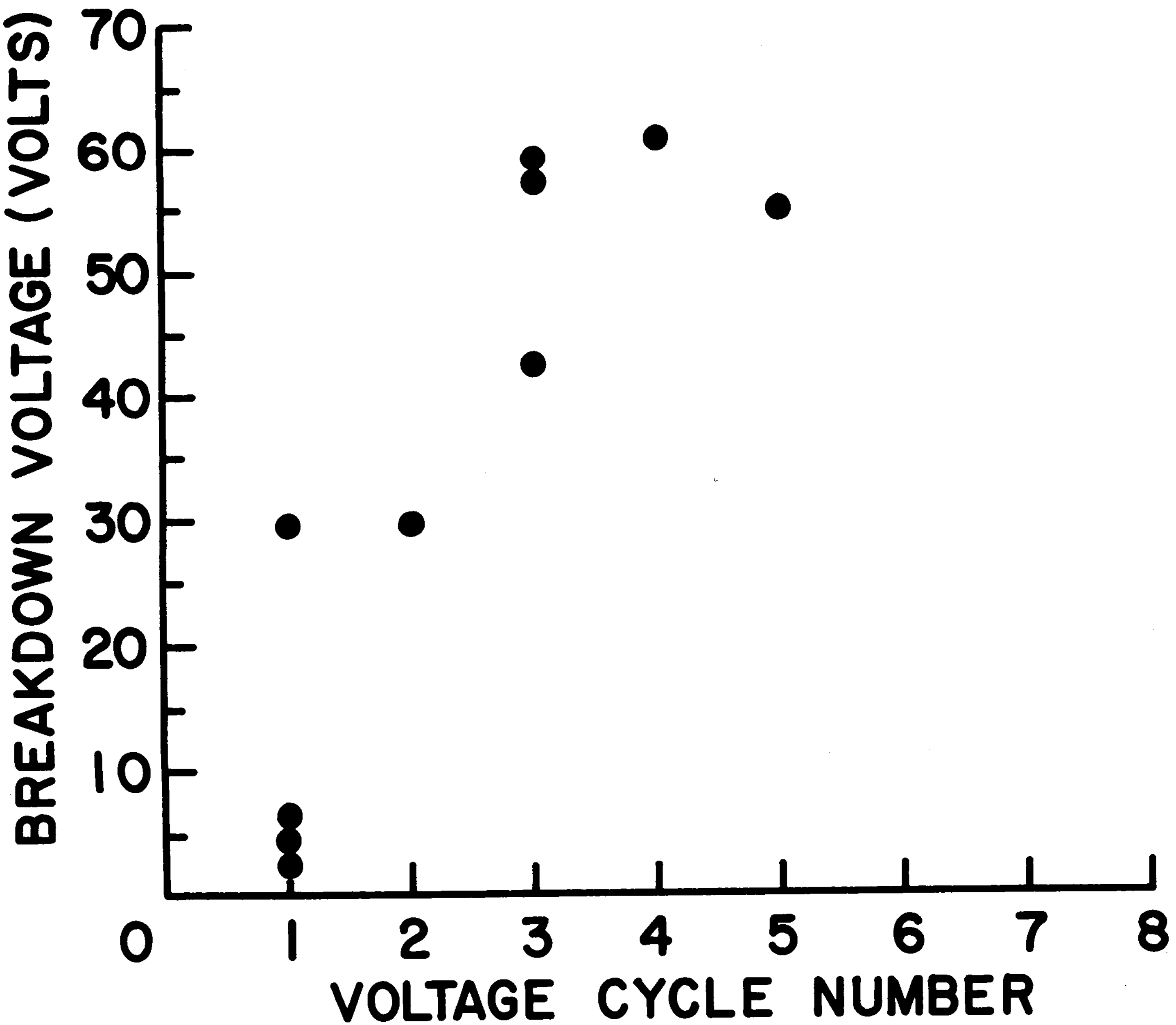

Fig. 7. Breakdown voltage versus current-voltage cycle for capacitor Pr-1-A.

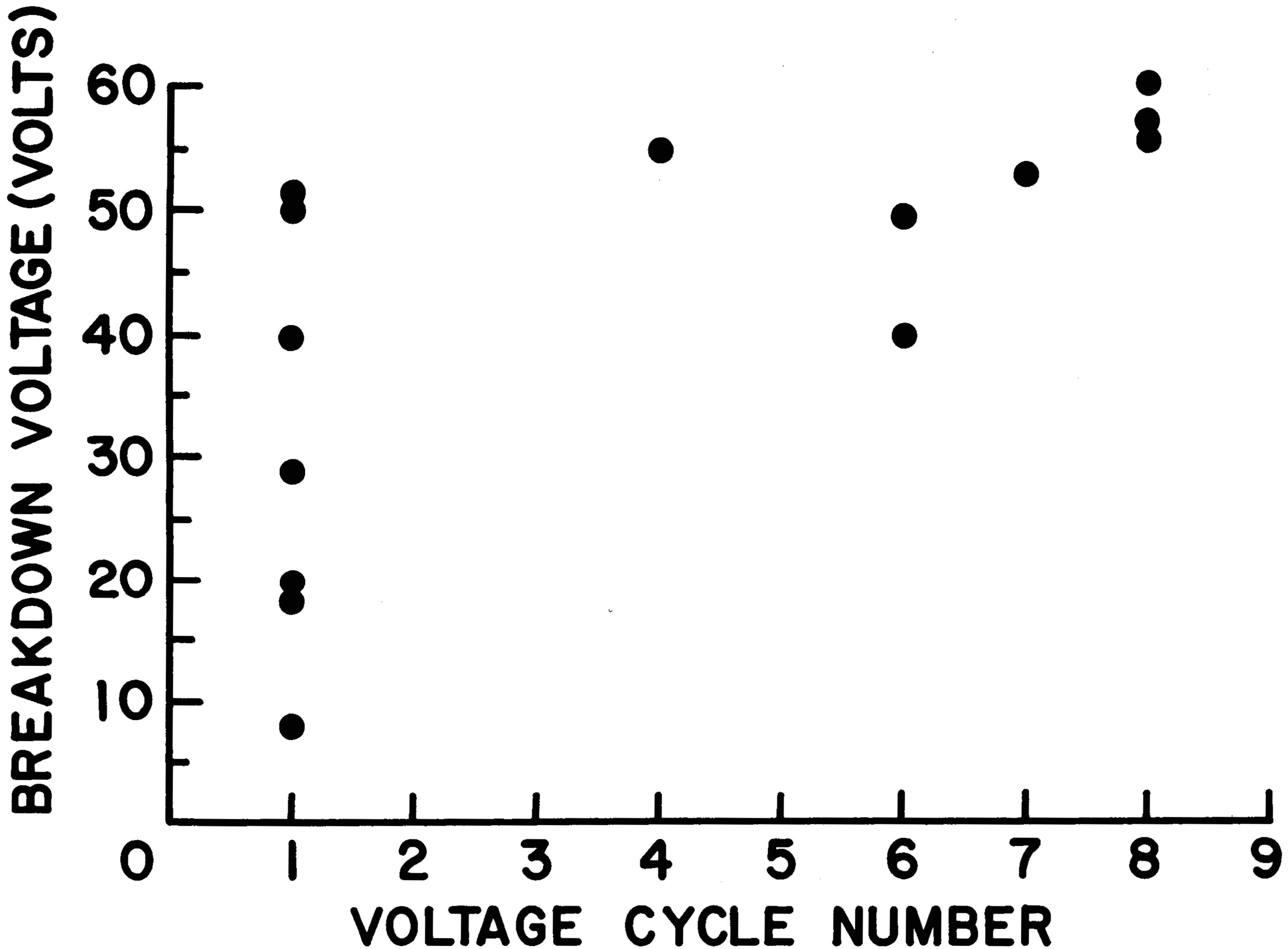

Fig. 8. Breakdown voltage versus current-voltage cycle for capacitor Nd-1-A.

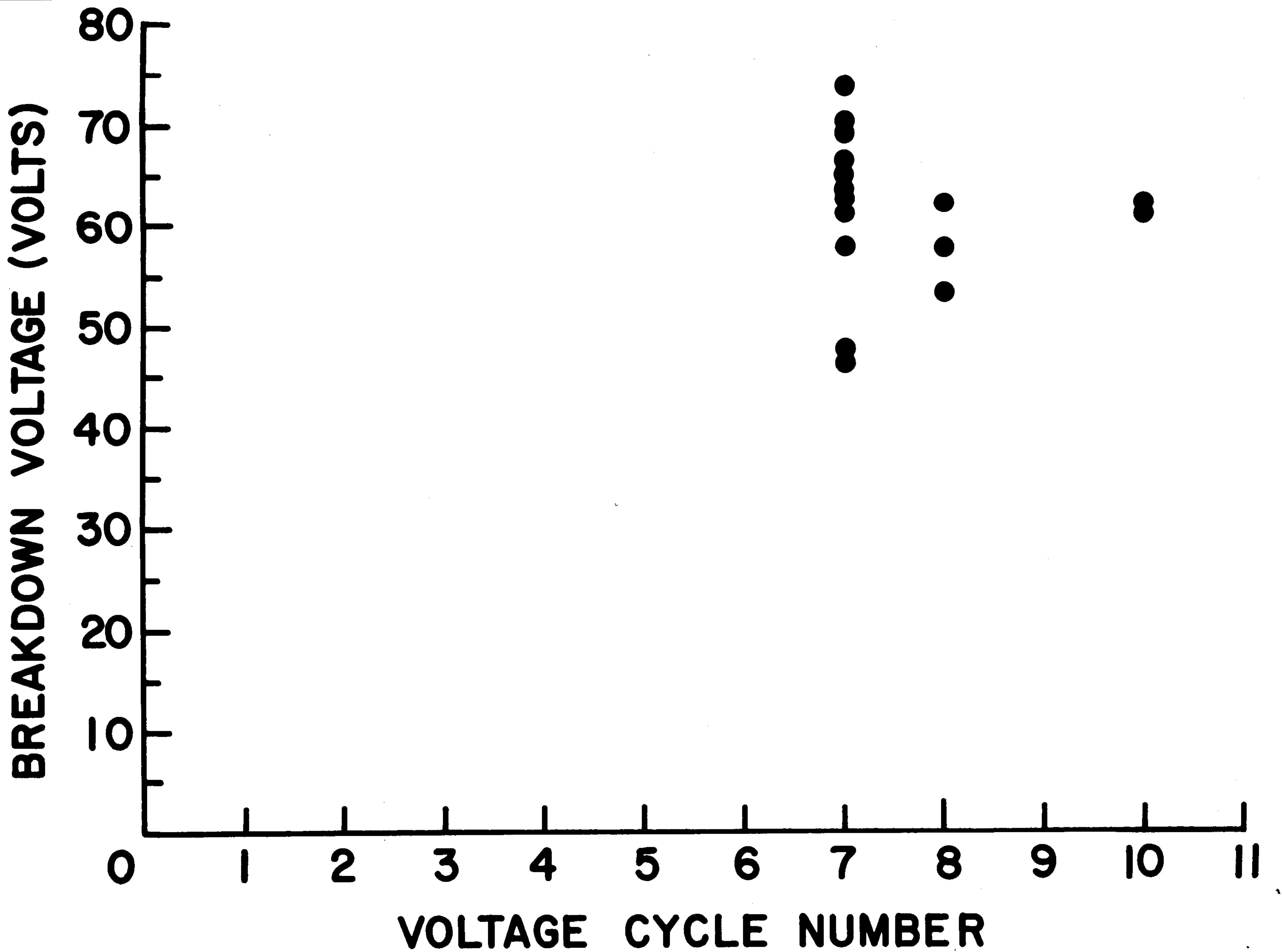

Fig. 9. Breakdown voltage versus current-voltage cycle for capacitor Gd-1-A.

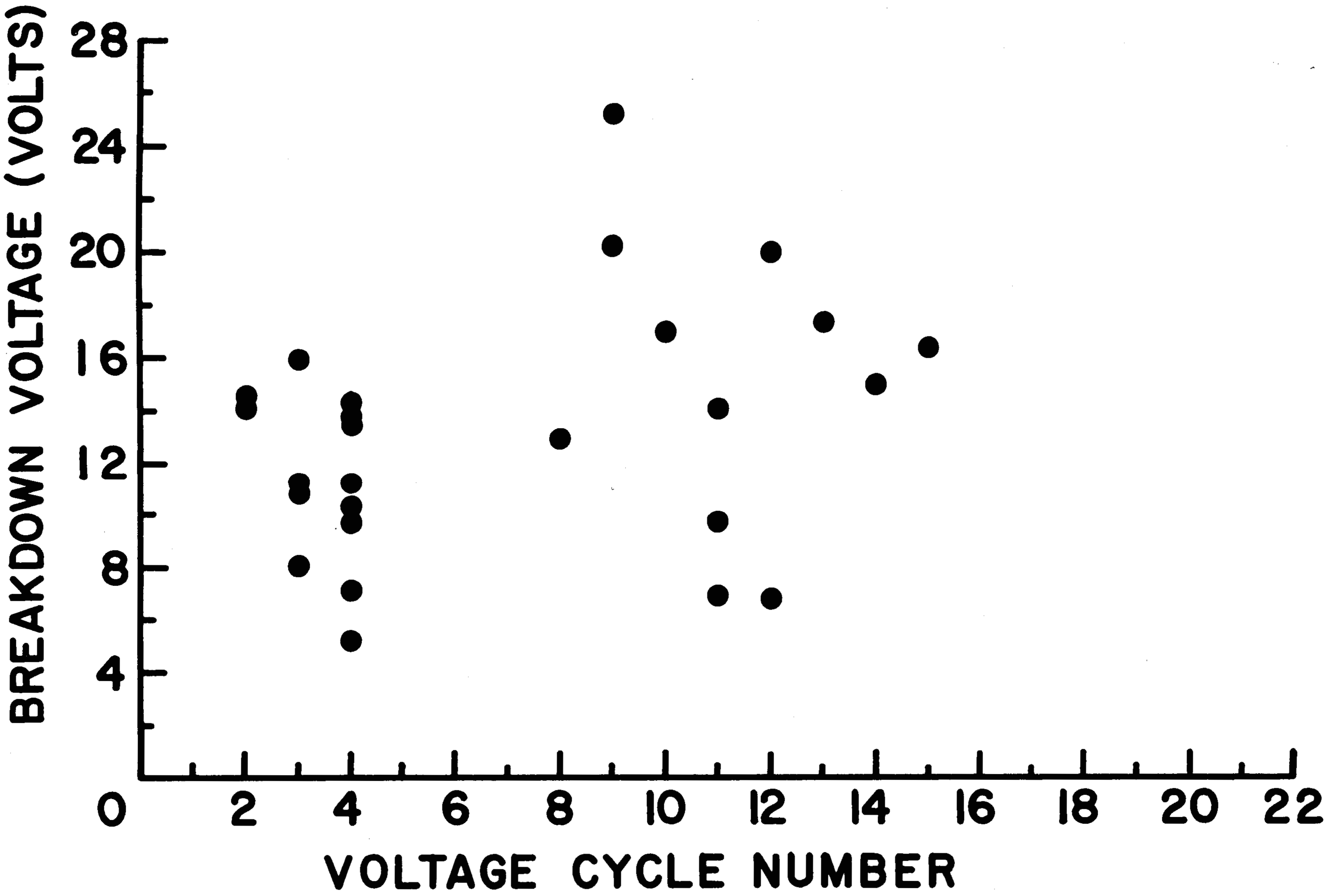

Fig. 10. Breakdown voltage versus current-voltage cycle for capacitor Dy-1-A.

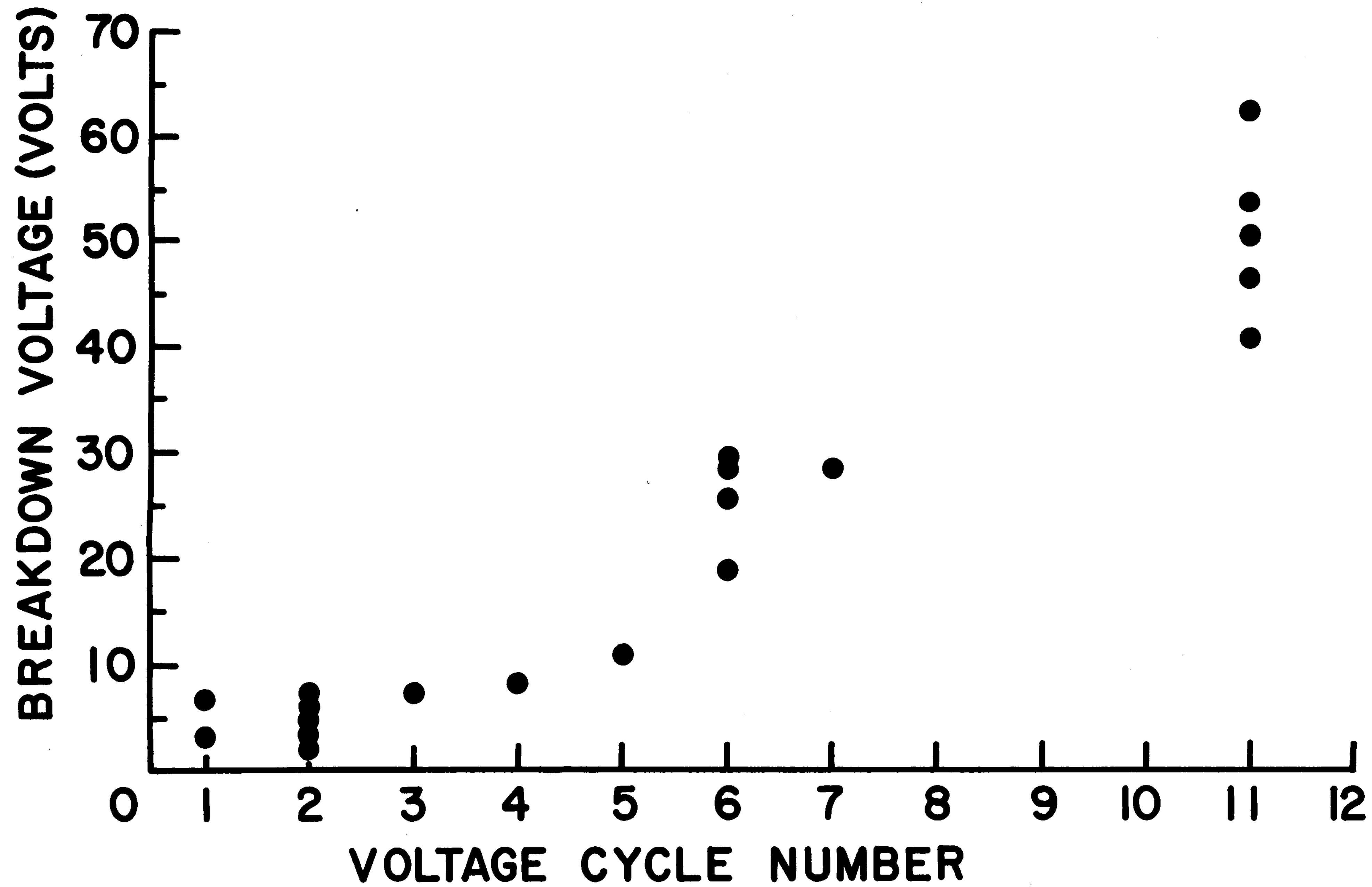

Fig. 11. Breakdown voltage versus current-voltage cycle for capacitor Ho-3-A.

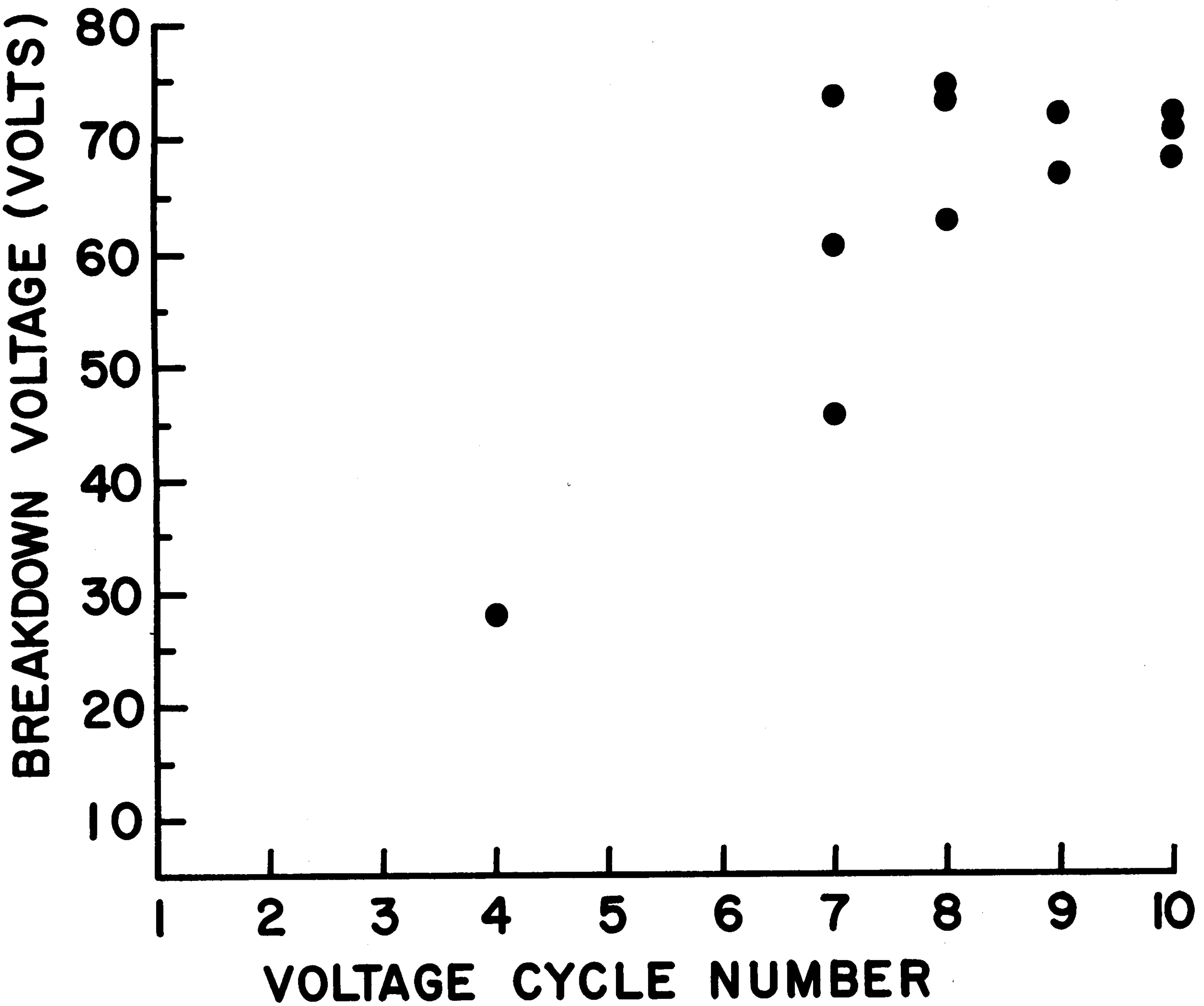

Fig. 12. Breakdown voltage versus current-voltage cycle for capacitor Er-1-B.

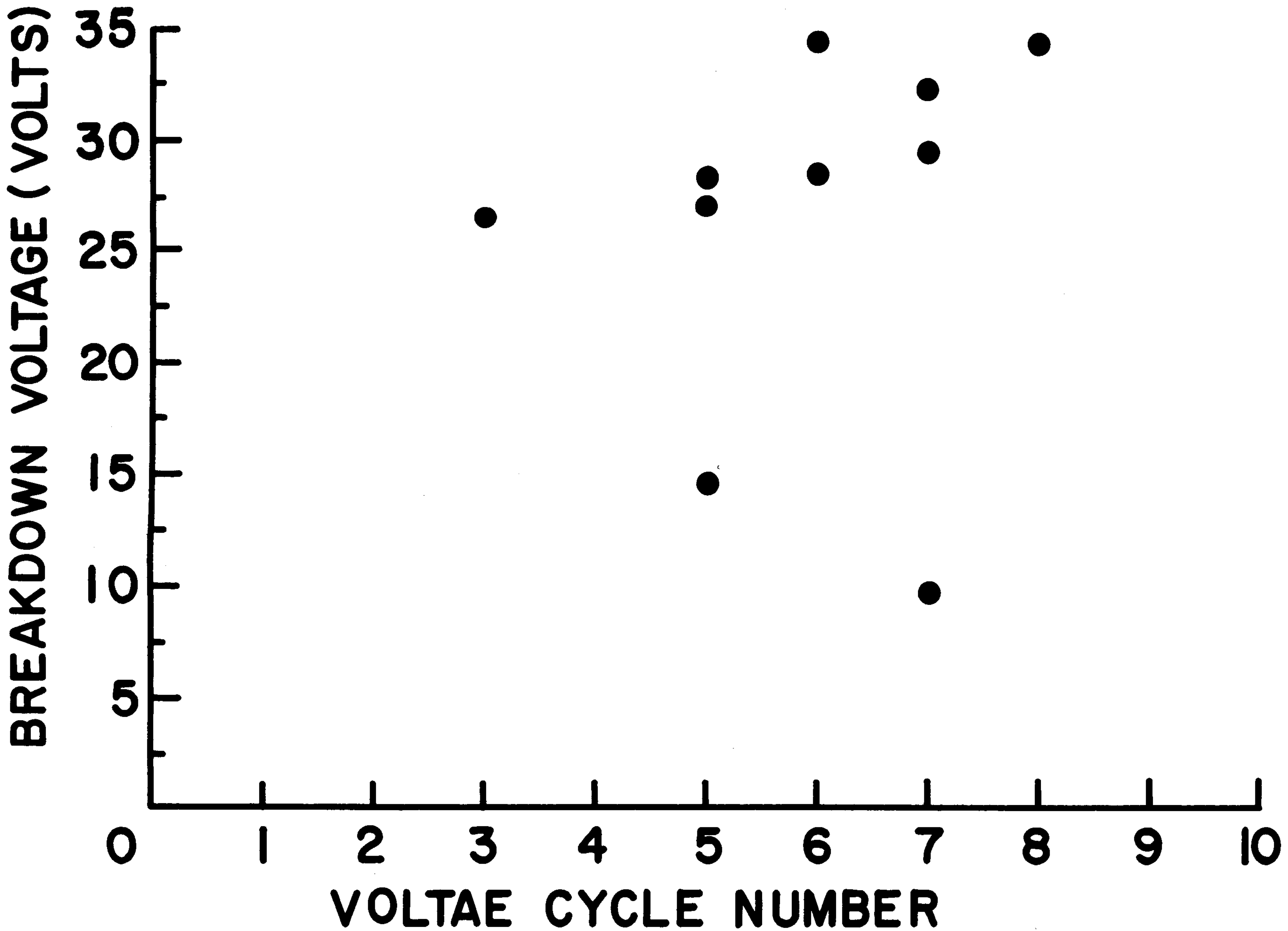

Fig. 13. Breakdown voltage versus current-voltage cycle for capacitor Yb-1-A.

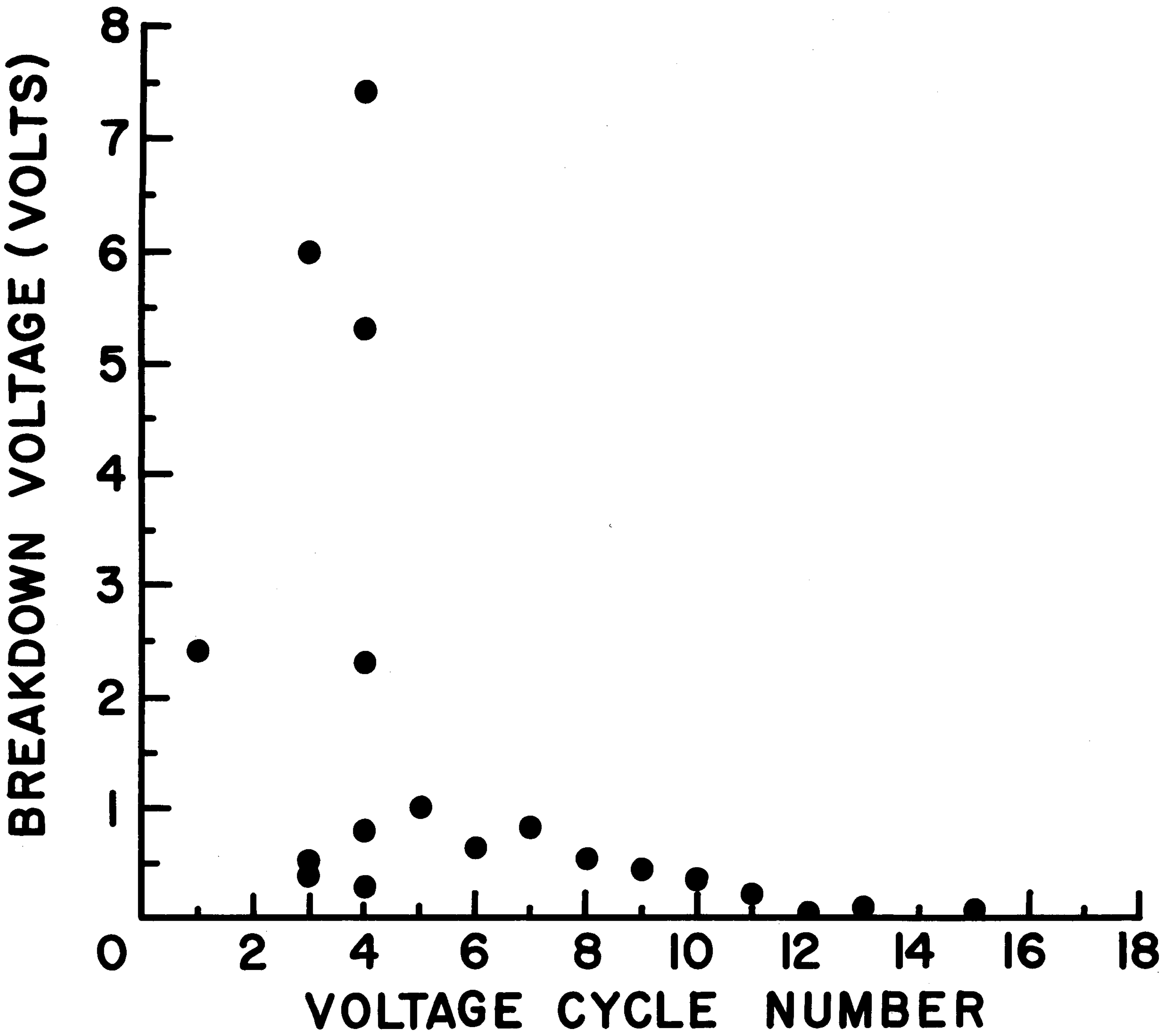

Fig. 14. Breakdown voltage versus current-voltage cycle for capacitor Sc-1-A.

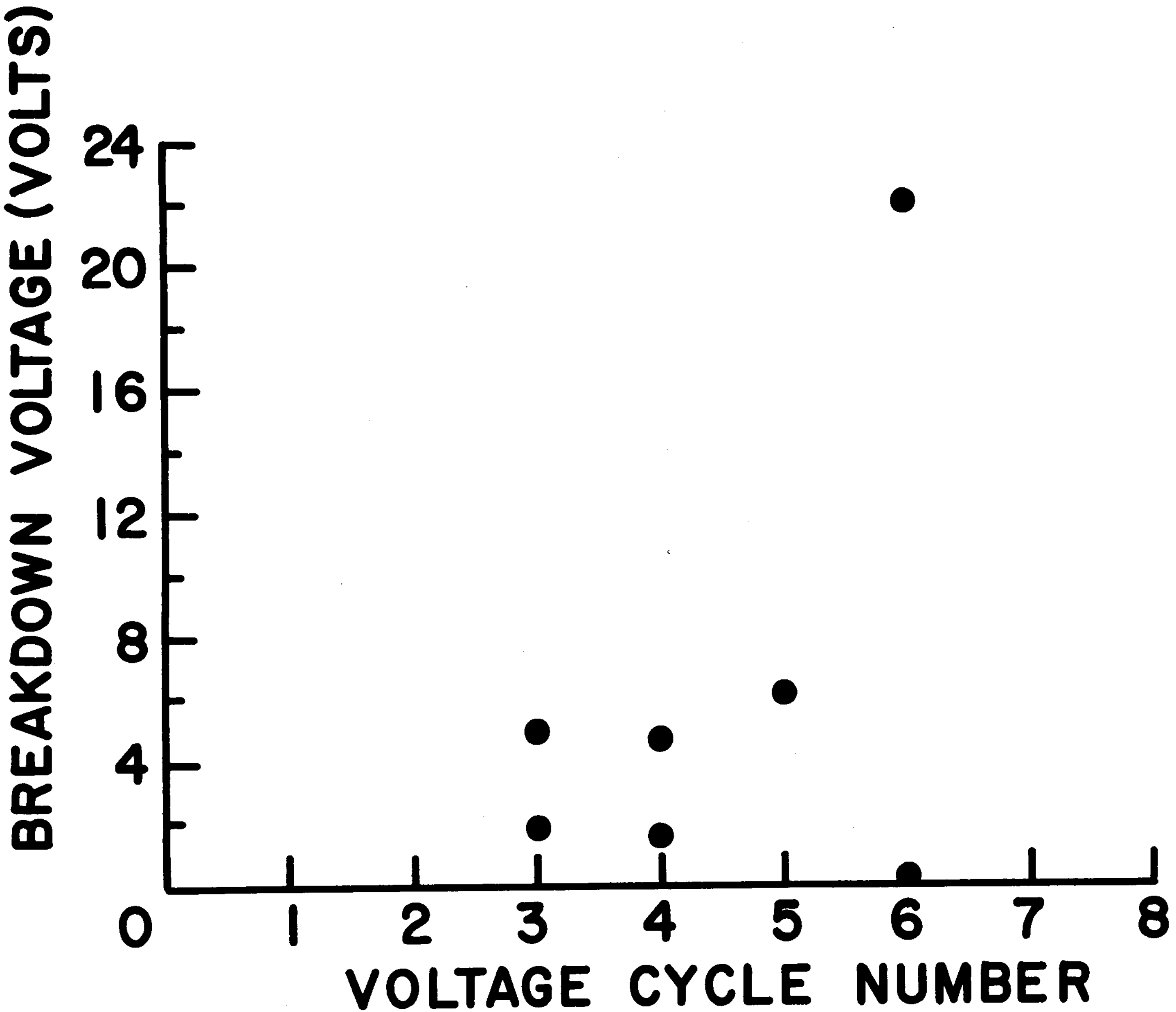

Fig. 15. Breakdown voltage versus current-voltage cycle for capacitor Y-1-C.

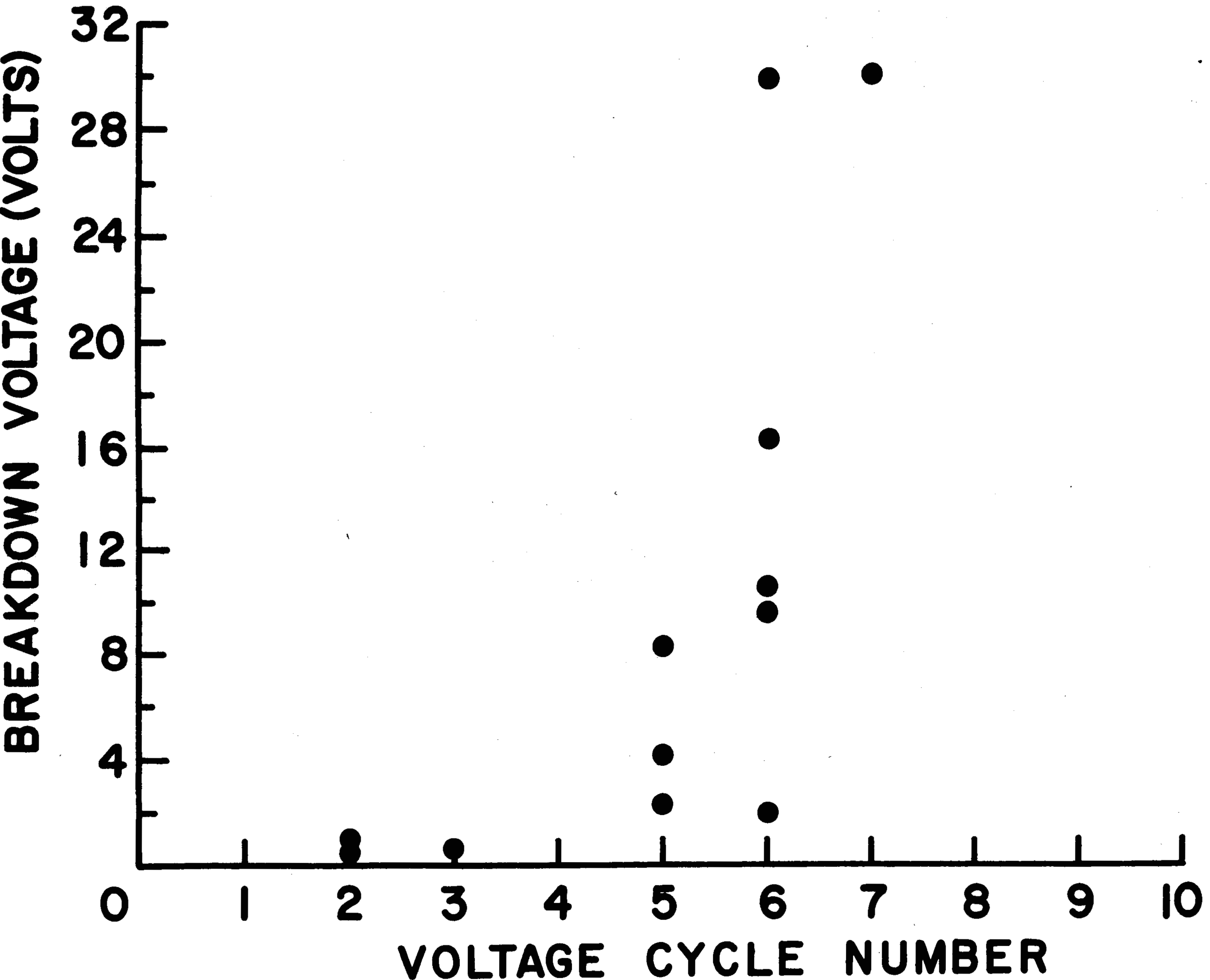

Fig. 16. Breakdown voltage versus current-voltage cycle for capacitor Sm-1-A.

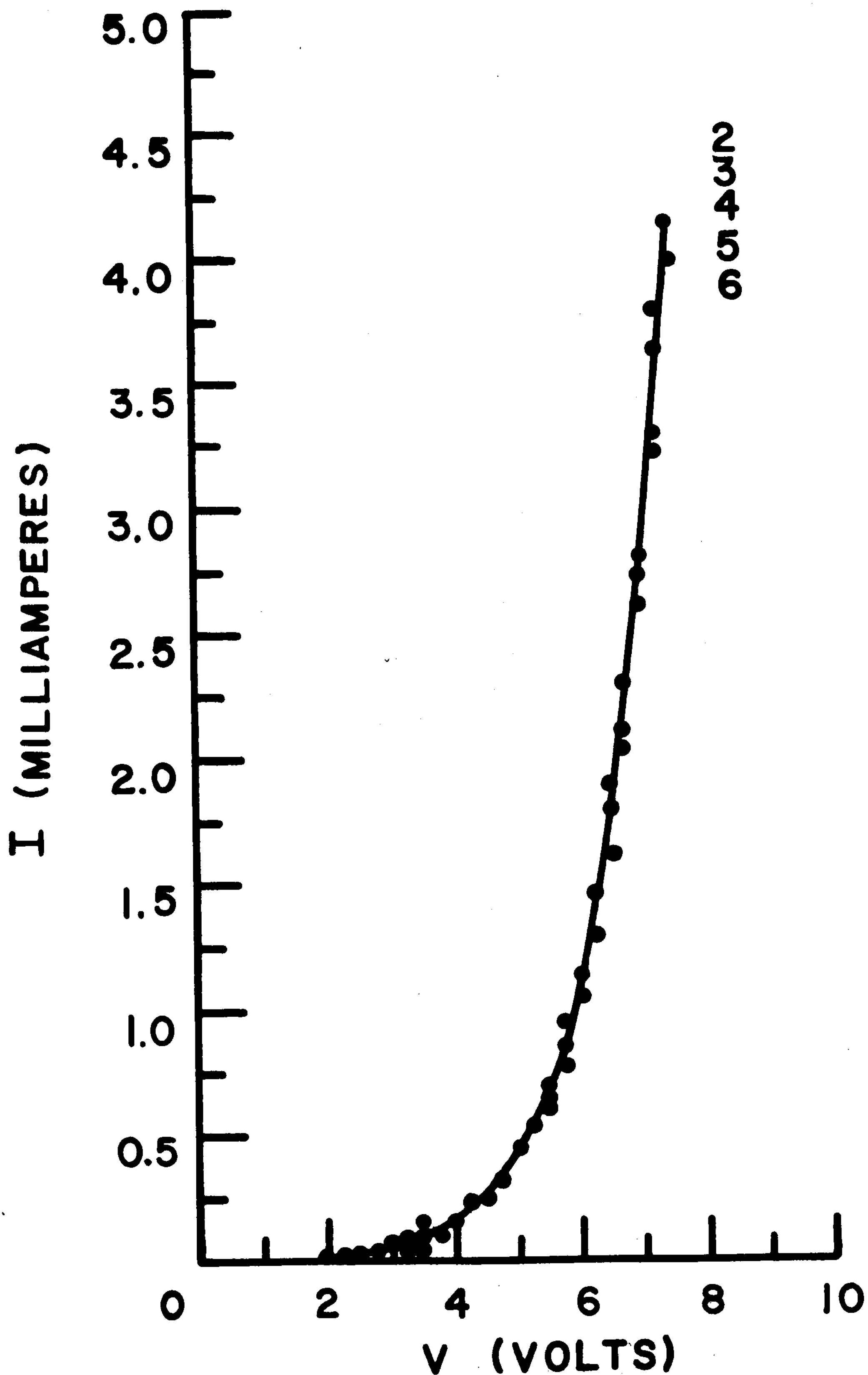

Fig. 17. Steady-state current-voltage characteristics for capacitor Gd-3-D (oxide film thickness 1465 Å) at a pressure of 1×10^{-6} torr illustrating consistency for a number of current-voltage cycles. (The numbers on the curves correspond to the current-voltage cycle.)

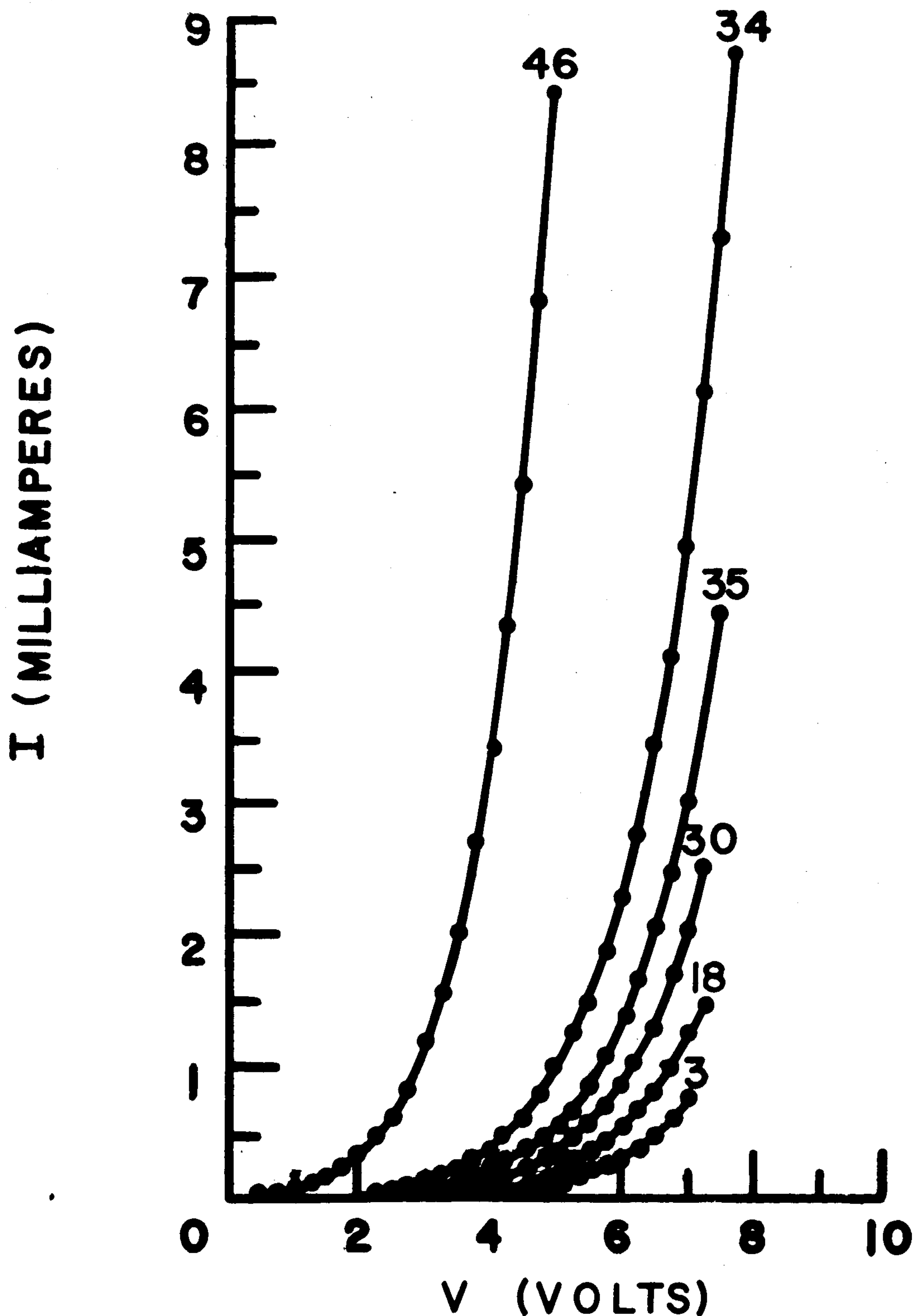

Fig. 18. Steady-state current-voltage characteristics for capacitor Gd-12-A (oxide film thickness 1494 Å) at a pressure of 9×10^{-7} torr illustrating the forming process with current-voltage cycle.

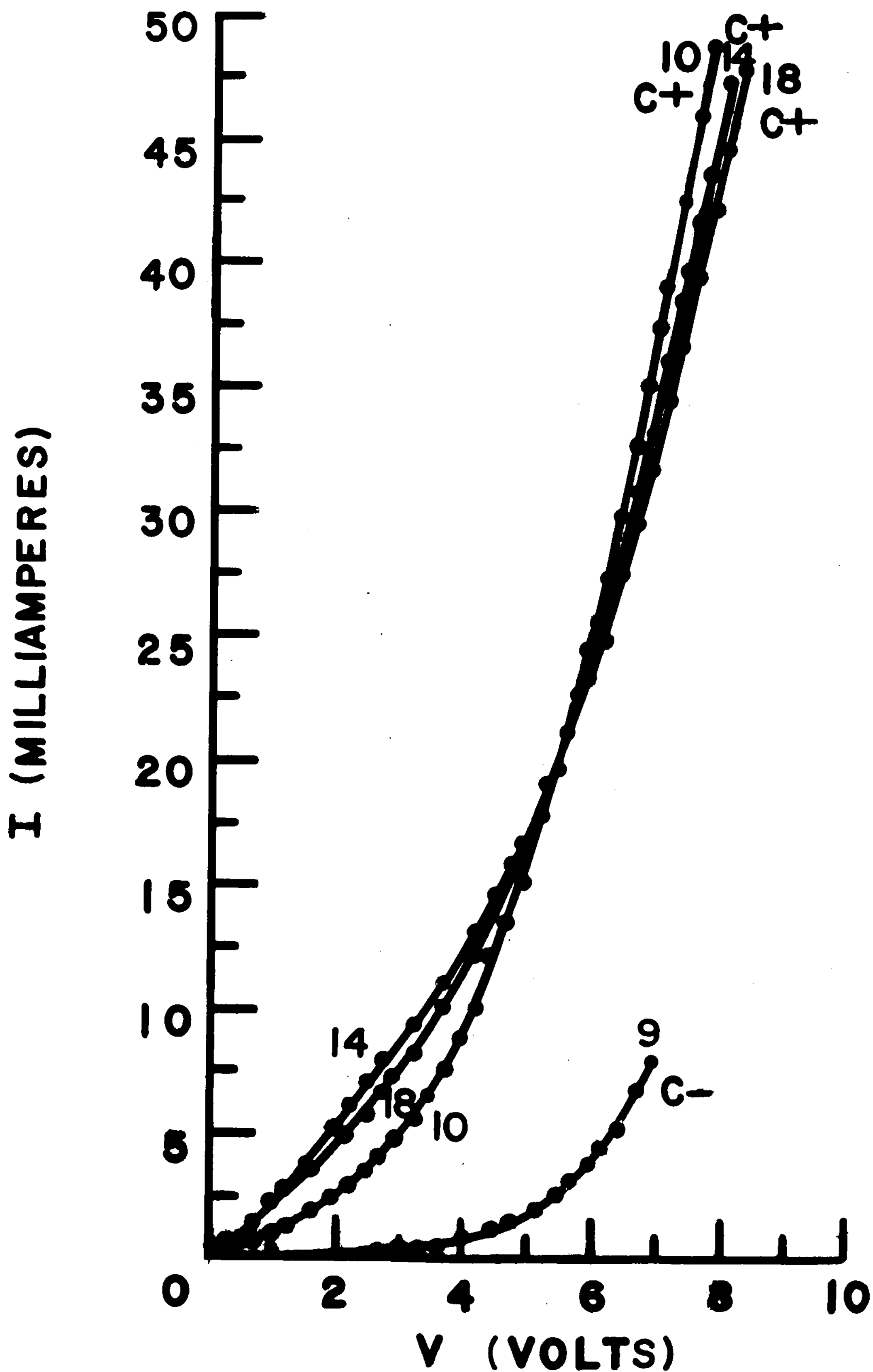

Fig. 19. Steady-state current-voltage characteristics for capacitor Gd-12-D (oxide film thickness 1494 Å) at a pressure of 8.2×10^{-7} torr illustrating the forming process and polarity effects. (Polarity is measured with respect to the bottom electrode.)

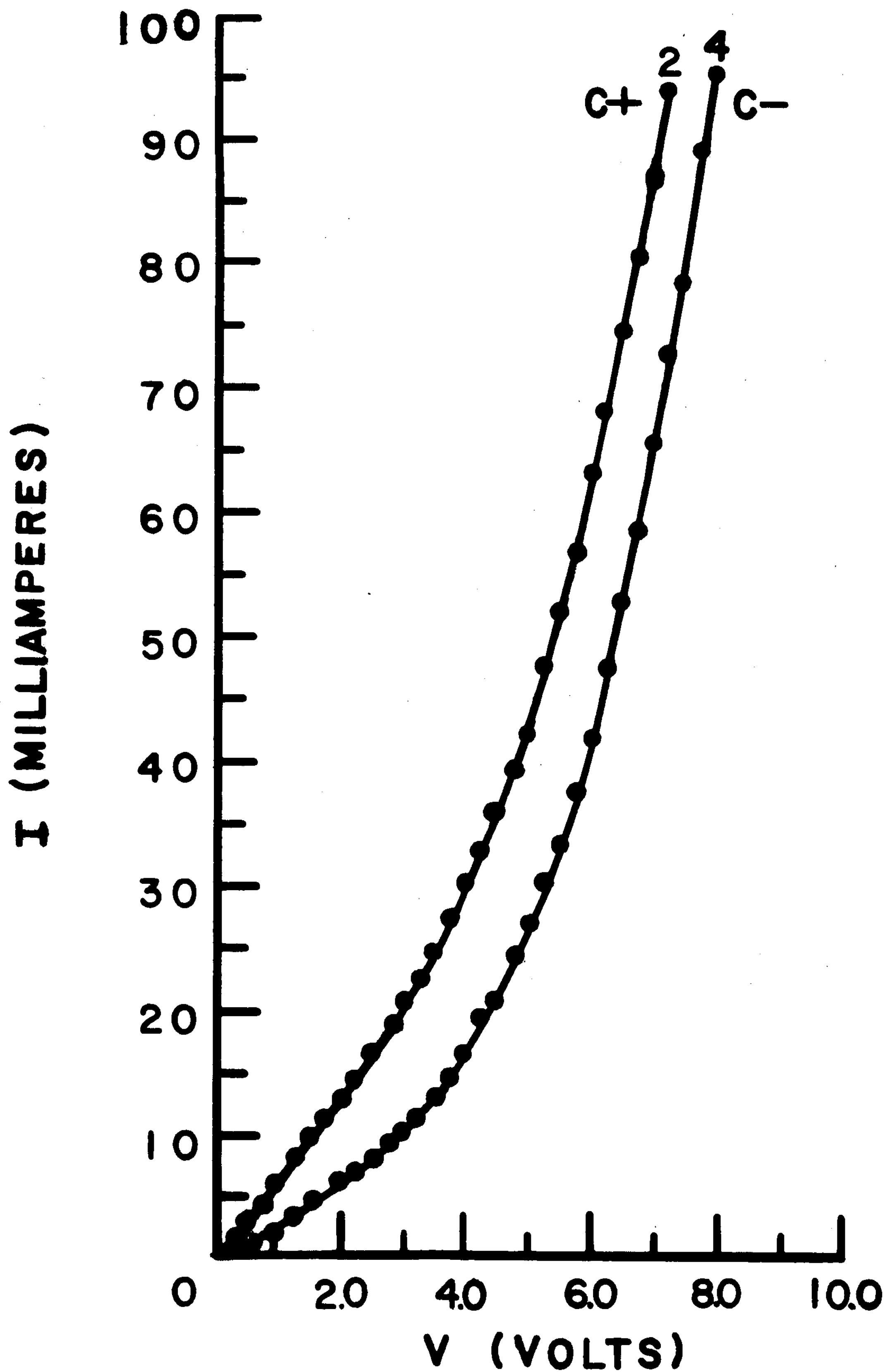

Fig. 20. Steady-state current-voltage characteristics for capacitor Gd-17-B (thickness unknown) at a pressure of 8×10^{-7} torr illustrating polarity effects.

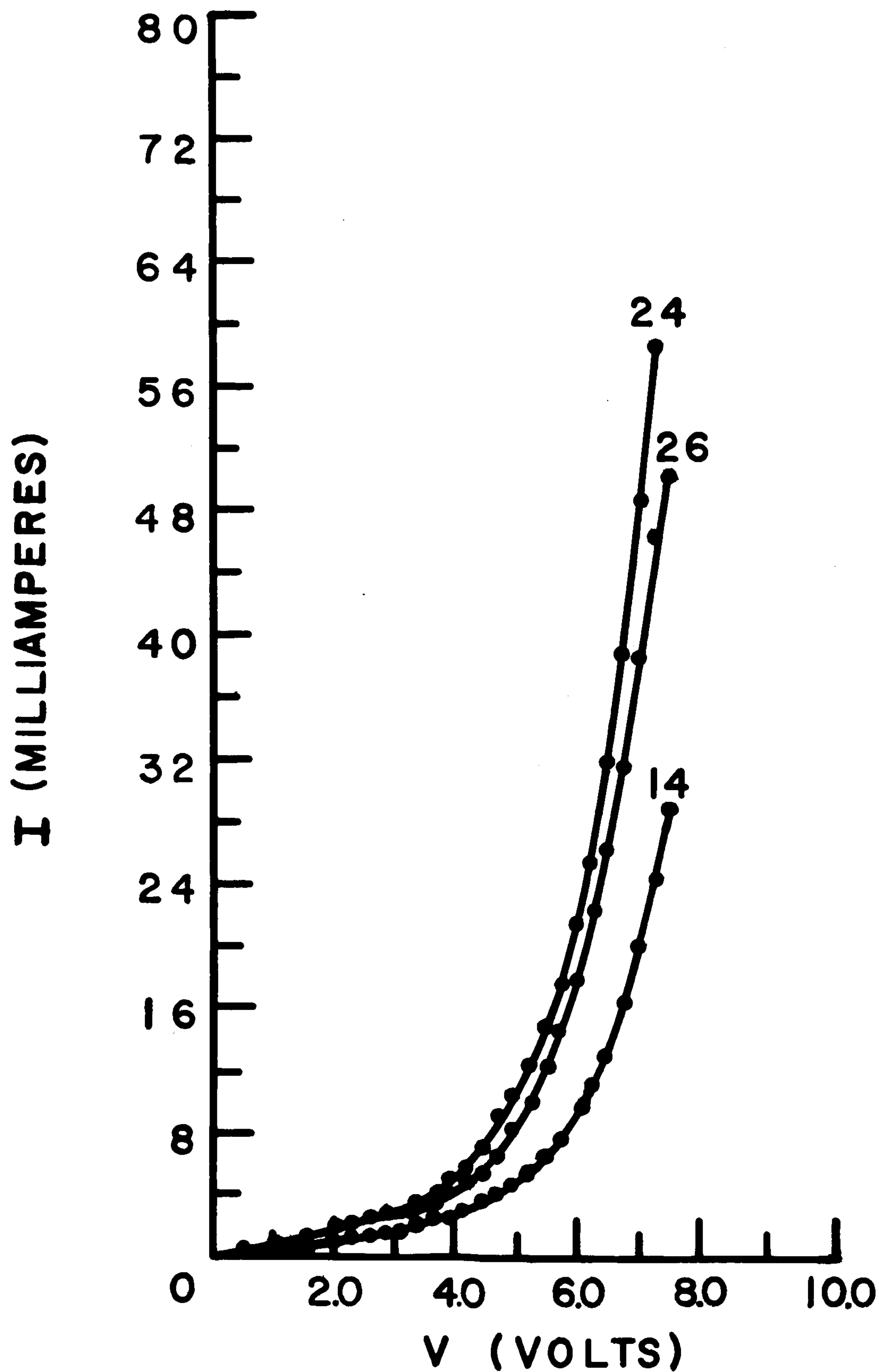

Fig. 21. Steady-state current-voltage characteristics for capacitor Nd-12-B (oxide film thickness 2295 Å) at a pressure of 1.6×10^{-6} torr illustrating the forming process with current-voltage cycle.

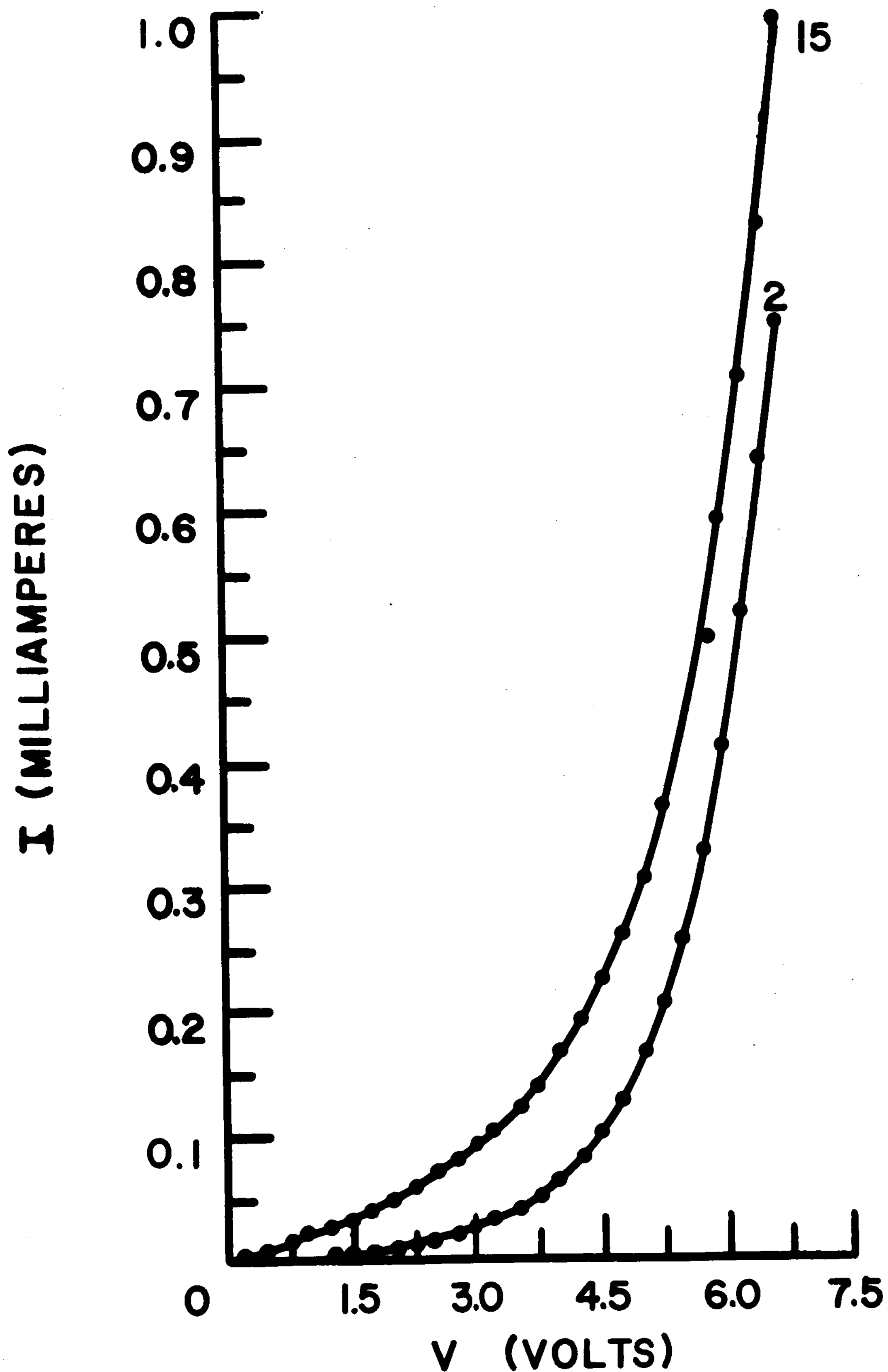

Fig. 22. Steady-state current-voltage characteristics for capacitor Nd-12-D (oxide film thickness 2295 Å) at a pressure of 1.6×10^{-6} torr illustrating the forming process with current-voltage cycle.

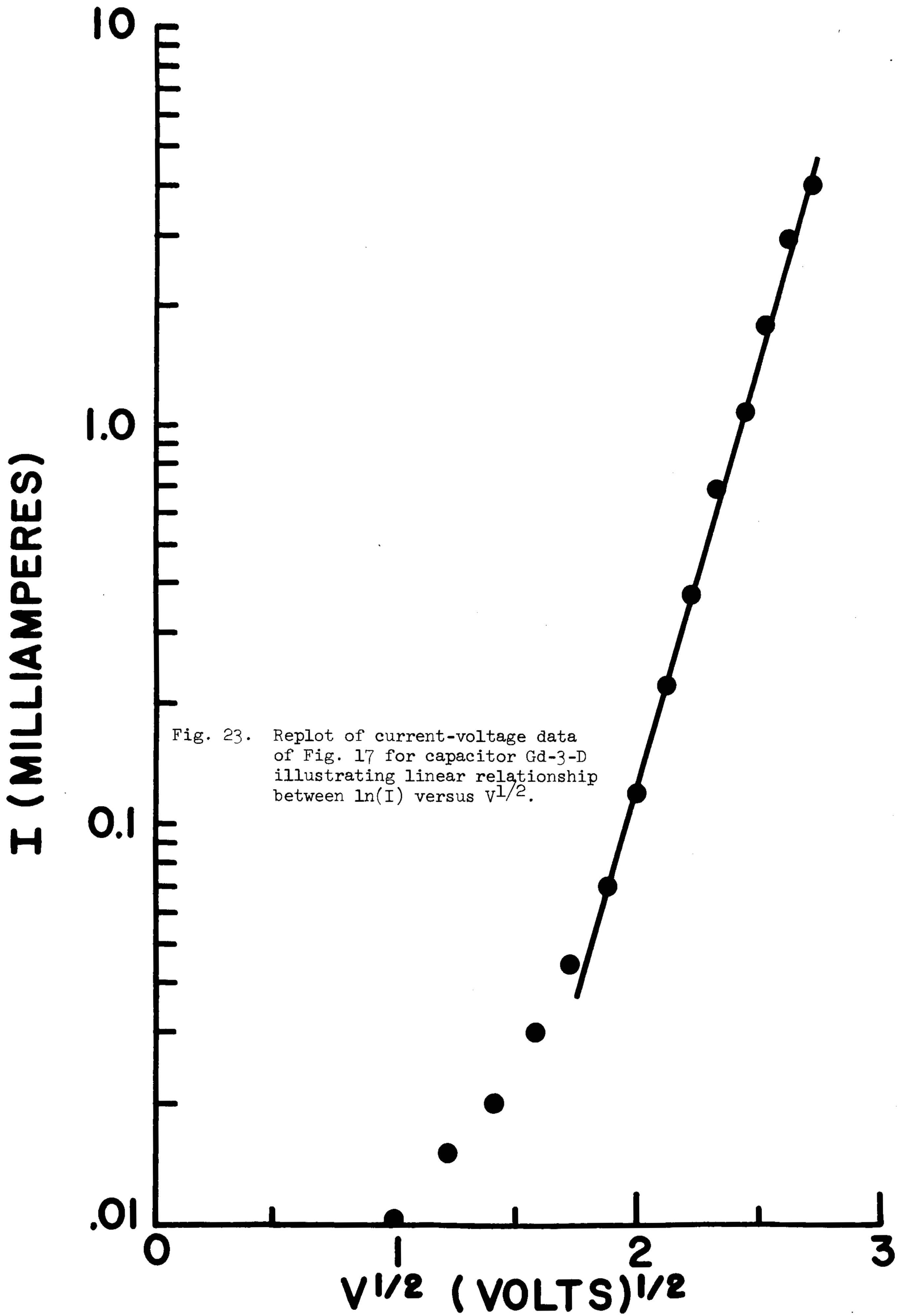

Fig. 23. Replot of current-voltage data of Fig. 17 for capacitor Gd-3-D illustrating linear relationship between ln(I) versus $V^{1/2}$.

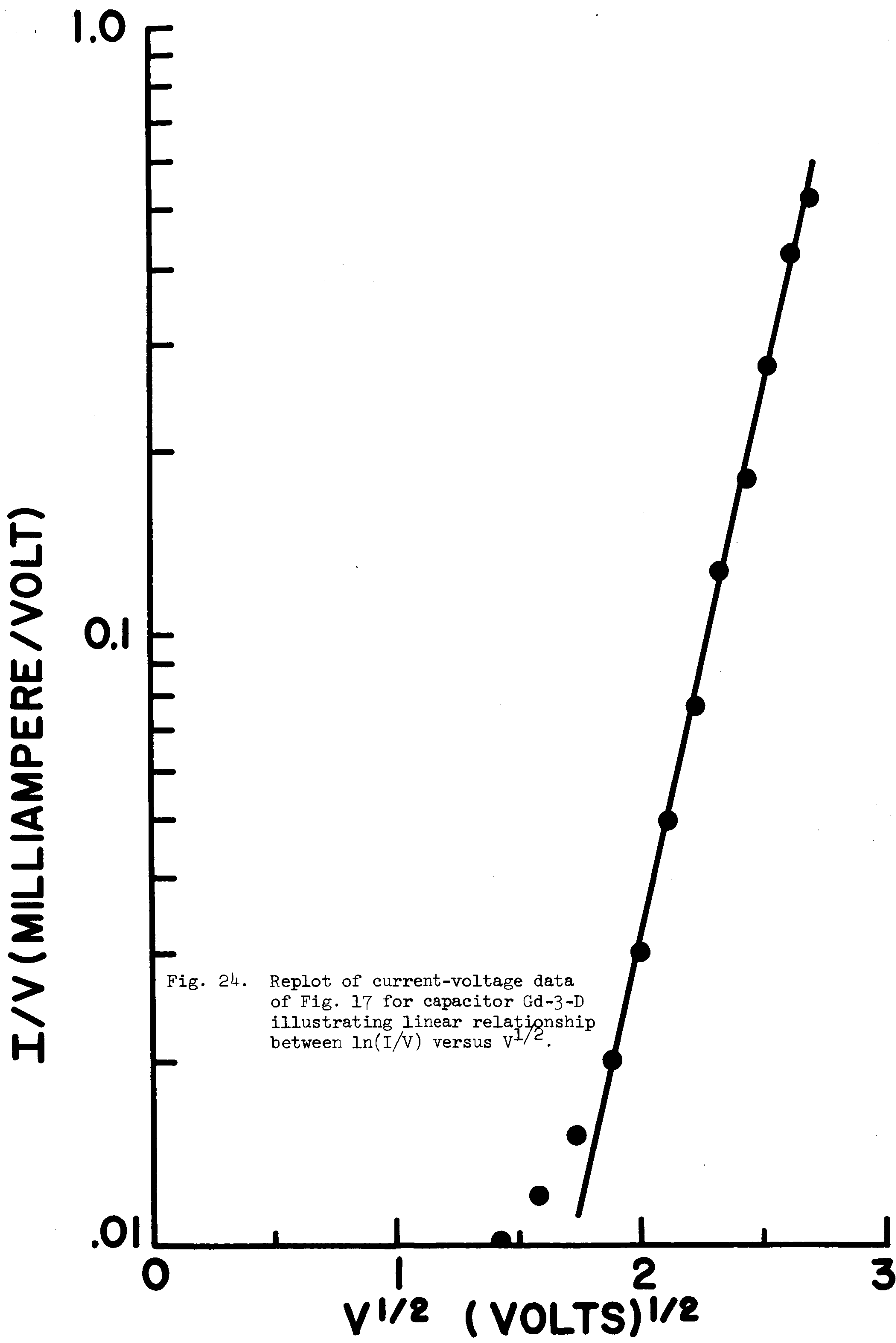

Fig. 24. Replot of current-voltage data of Fig. 17 for capacitor Gd-3-D illustrating linear relationship between $\ln(I/V)$ versus $V^{1/2}$.

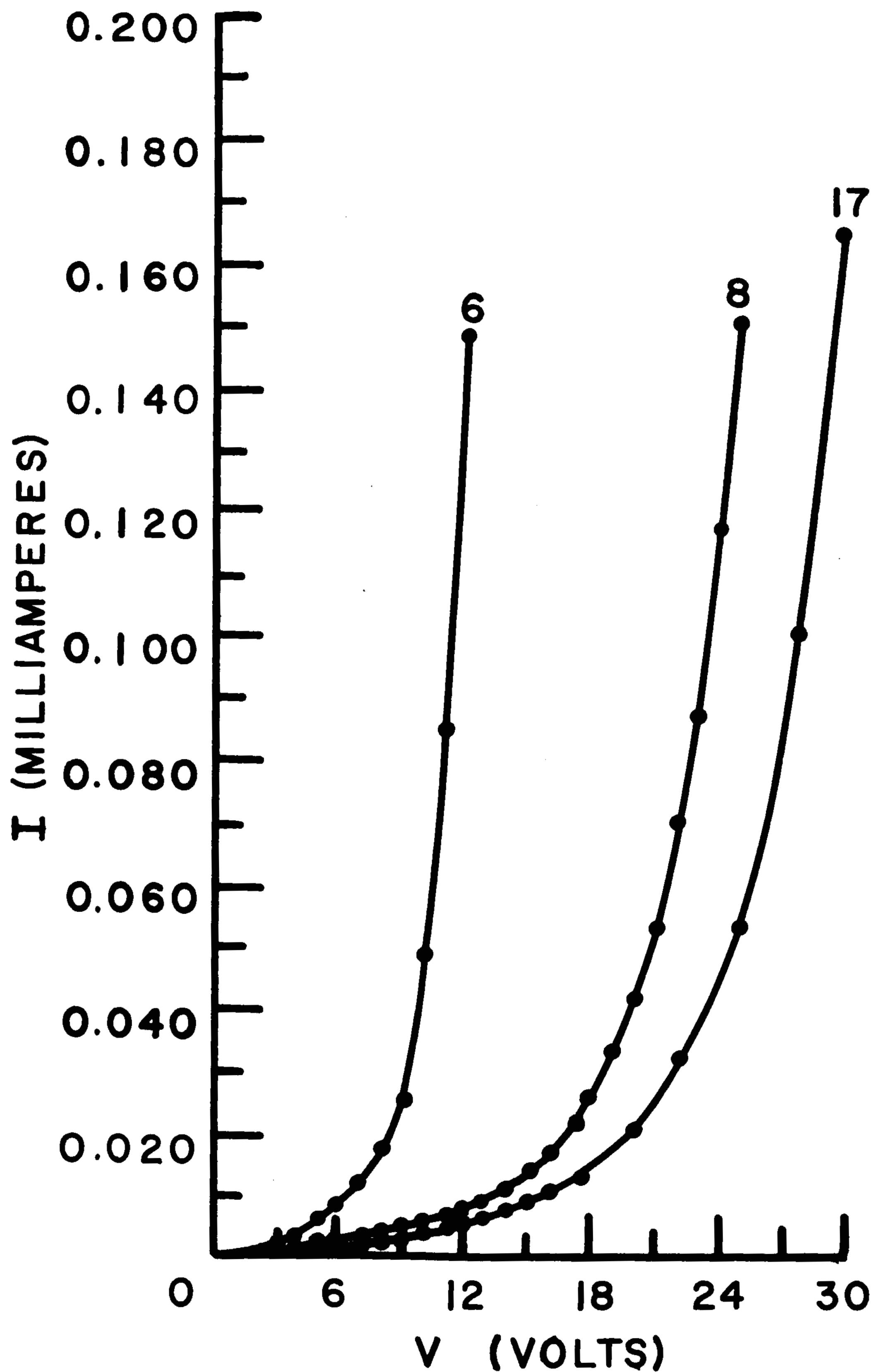

Fig. 25. Steady-state current-voltage characteristics for capacitor Nd-2-B (oxide film thickness 644 Å) at atmospheric pressure illustrating the forming process with current-voltage cycle.

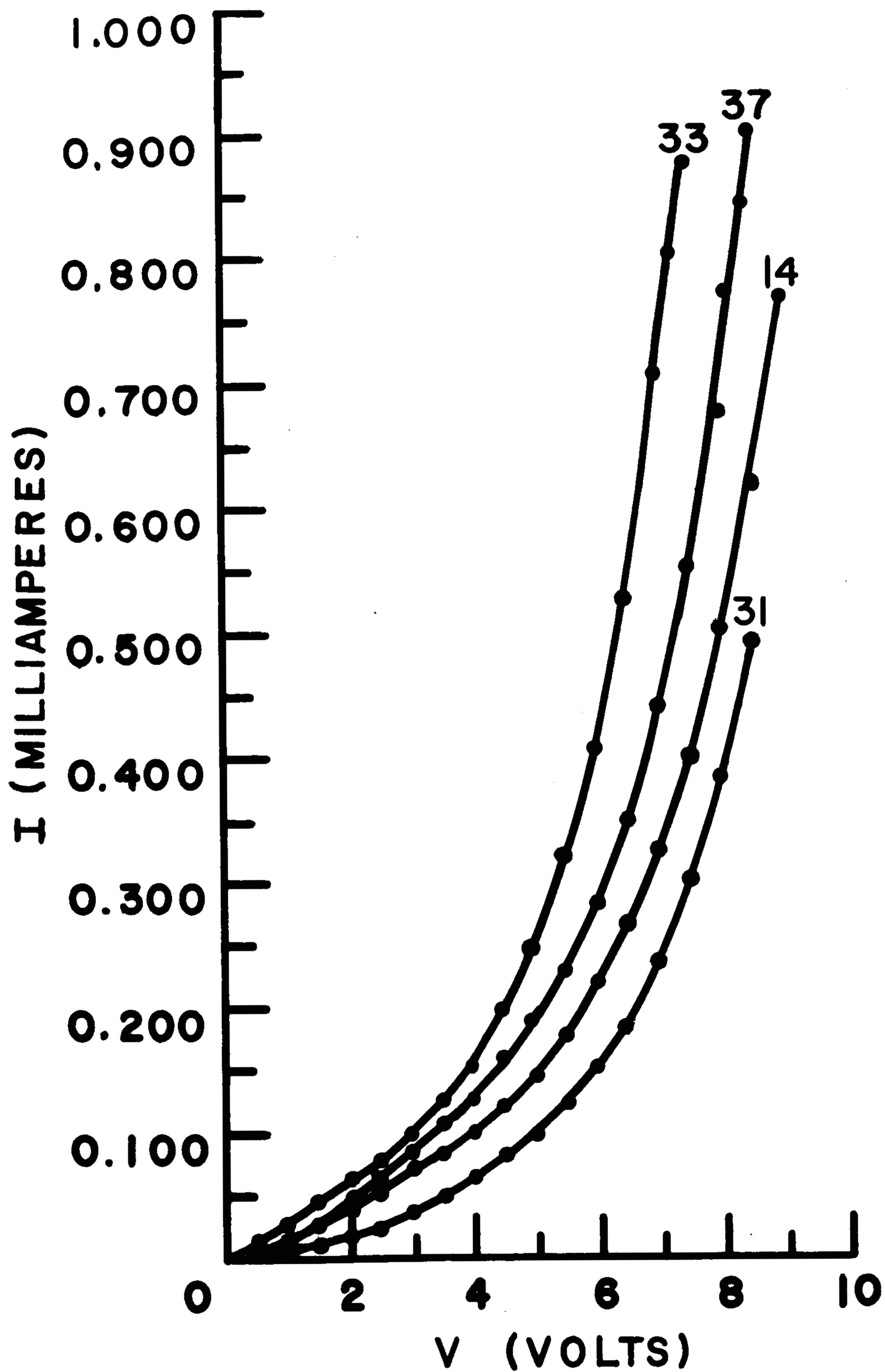

Fig. 26. Steady-state current-voltage characteristics for capacitor Nd-11-B (thickness unknown) at atmospheric pressure illustrating the forming process with current-voltage cycle.

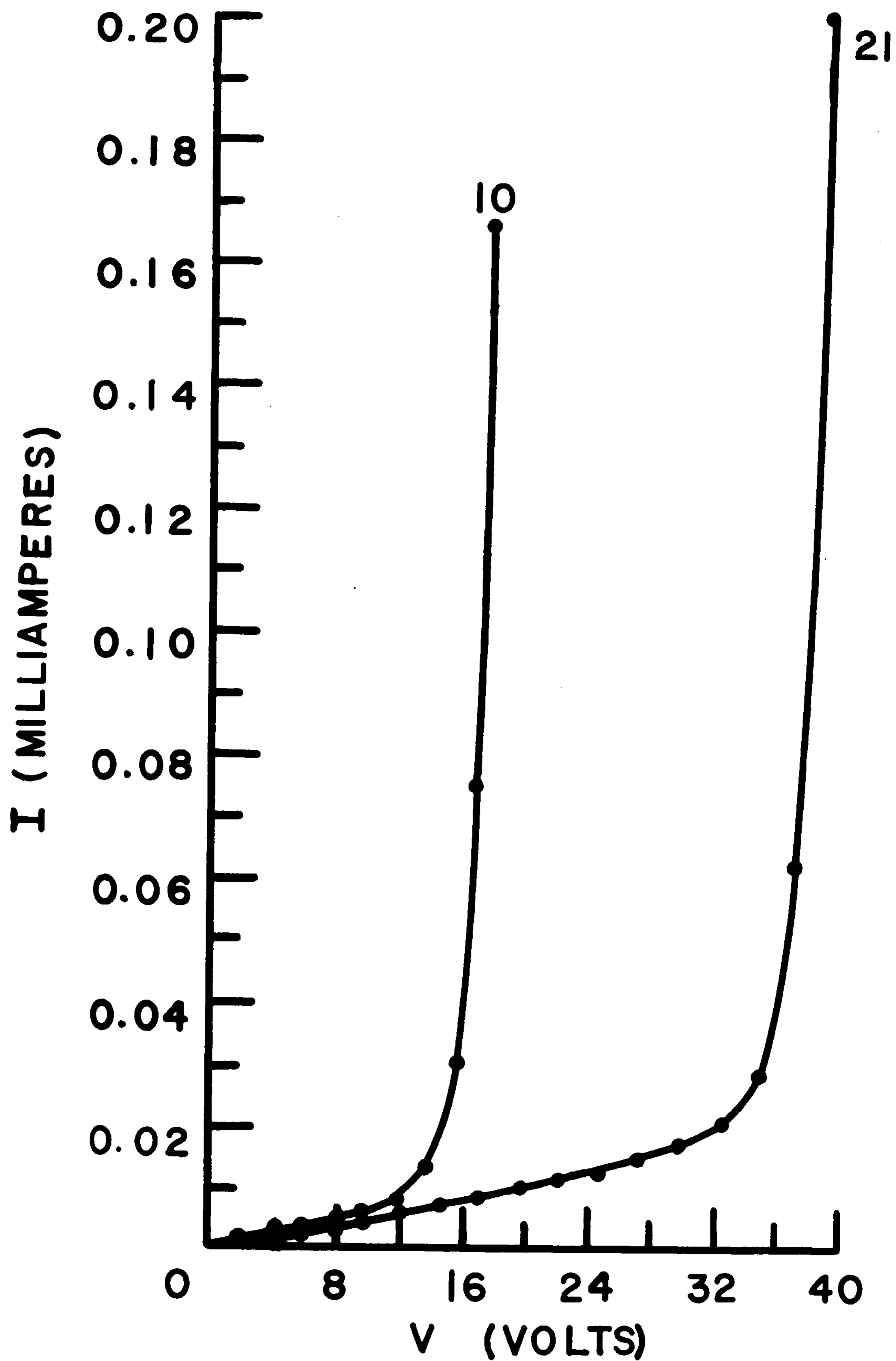

Fig. 27. Steady-state current-voltage characteristics for capacitor Er-2-B (thickness unknown) at atmospheric pressure.

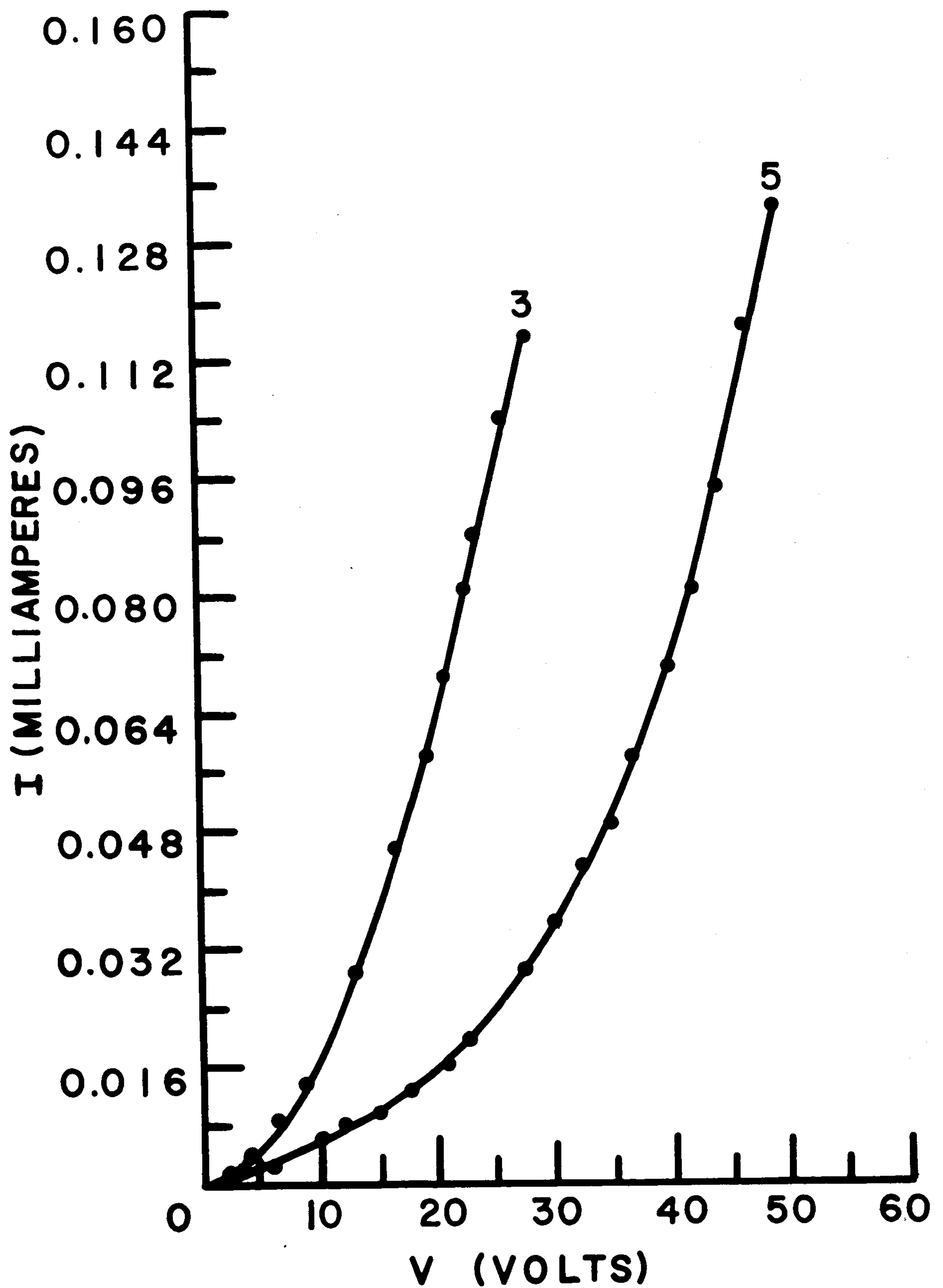

Fig. 28. Steady-state current-voltage characteristics for capacitor Ce-1-A (oxide film thickness 6440 Å) at atmospheric pressure.

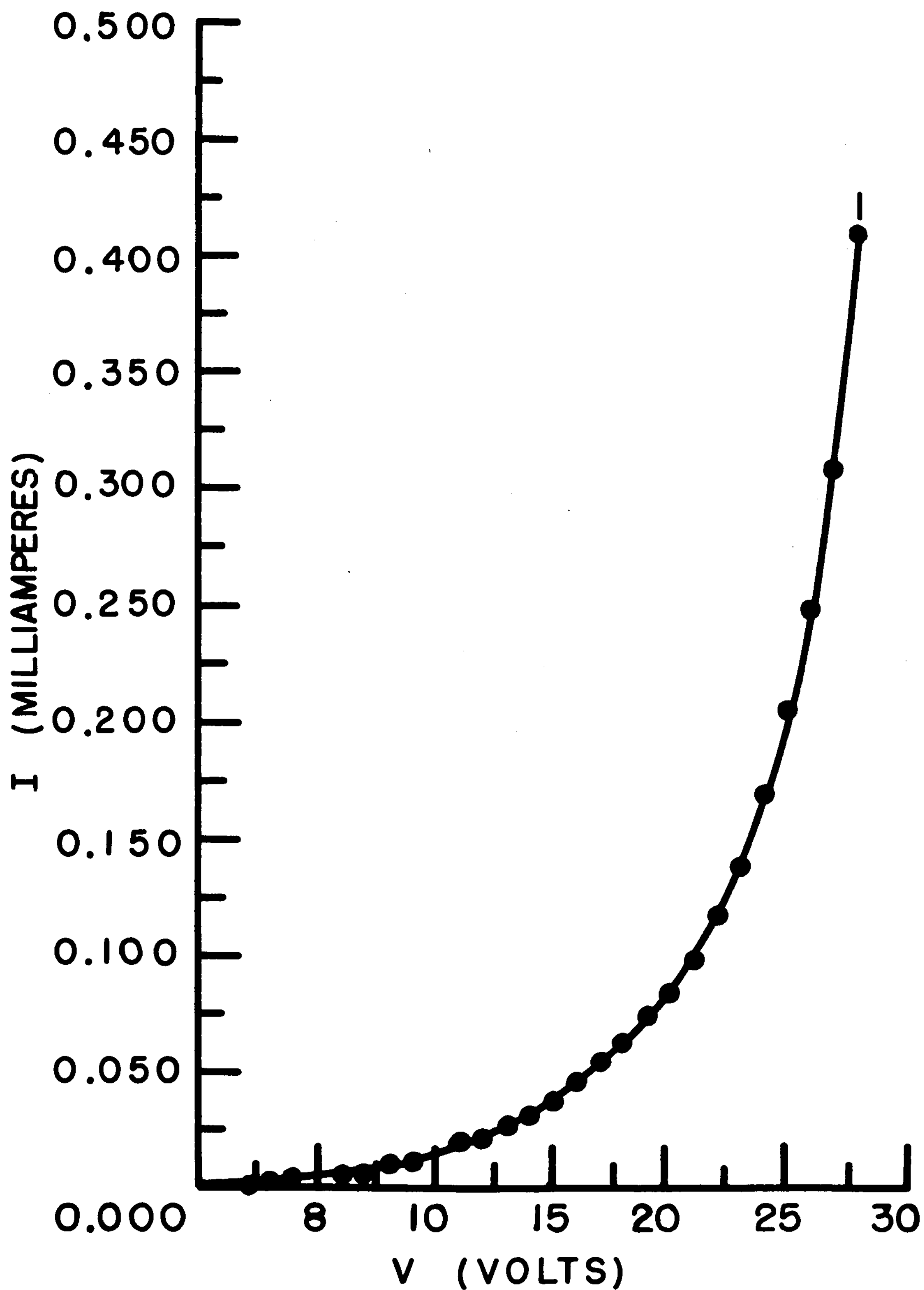

Fig. 29. Steady-state current-voltage characteristics for capacitor La-3-B (oxide film thickness approximately 322 Å) at atmospheric pressure.

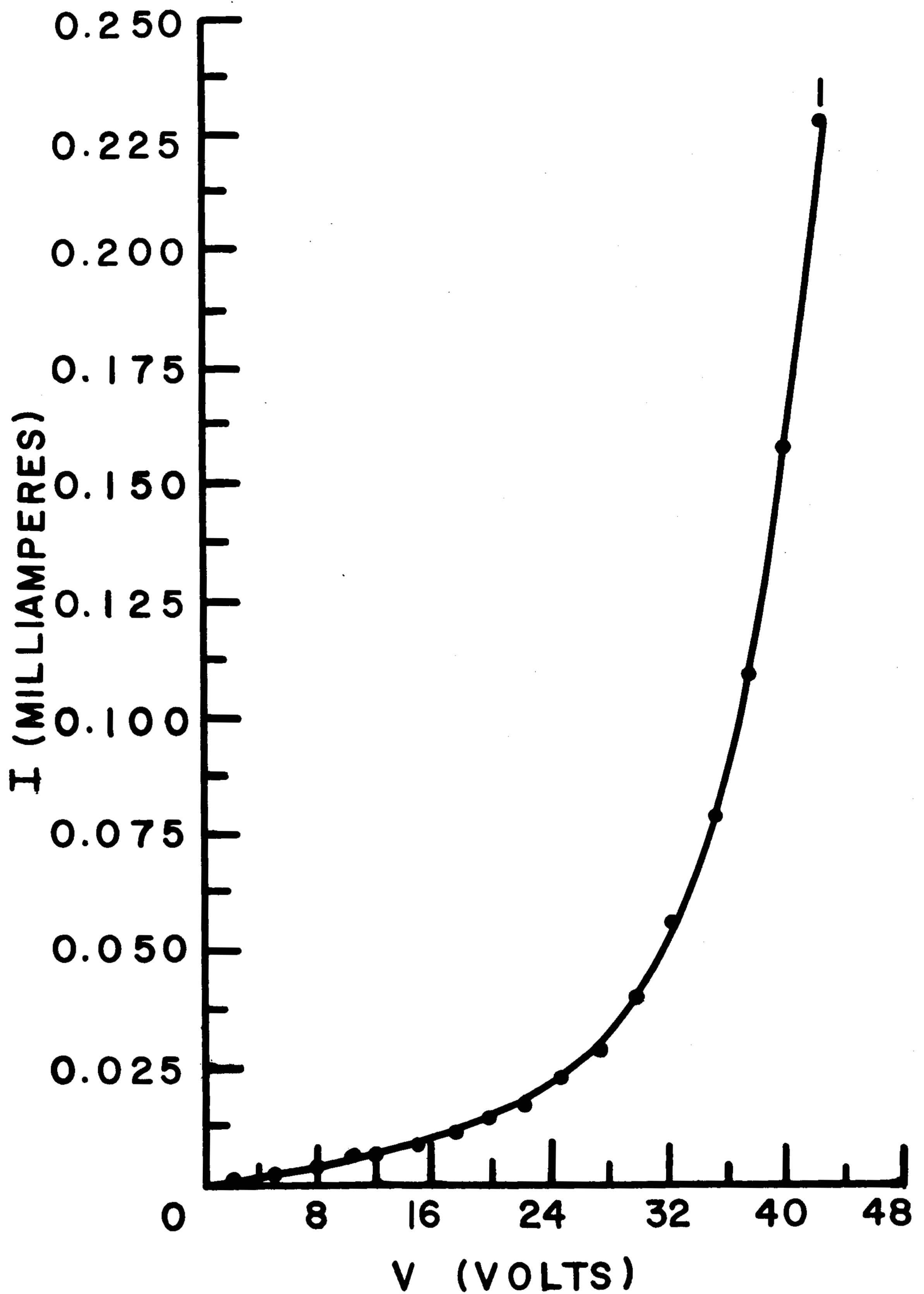

Fig. 30. Steady-state current-voltage characteristics for capacitor Pr-2-B (oxide film thickness 1288 Å) at atmospheric pressure.